Coordinated Control of an Underwater Glider Fleet in an Adaptive Ocean Sampling Field Experiment in Monterey Bay

Naomi E. Leonard
Mechanical and Aerospace Engineering, Princeton University, Princeton, New Jersey 08544
e-mail: naomi@princeton.edu
Derek A. Paley
Department of Aerospace Engineering, University of Maryland, College Park, Maryland 20742
e-mail: dpaley@umd.edu
Russ E. Davis
Physical Oceanography Research Division, Scripps Institution of Oceanography, La Jolla, California 92093
e-mail: rdavis@ucsd.edu
David M. Fratantoni
Physical Oceanography Department, Woods Hole Oceanographic Institution, Woods Hole, Massachusetts 02543
e-mail: dfratantoni@whoi.edu
Francois Lekien
Ecole Polytechnique, Université Libre de Bruxelles, Brussels, Belgium
e-mail: lekien@ulb.ac.be
Fumin Zhang
School of Electrical and Computer Engineering, Georgia Institute of Technology, Savannah, Georgia 31407
e-mail: fumin@gatech.edu

Received 25 January 2010; accepted 13 August 2010

A full-scale adaptive ocean sampling network was deployed throughout the month-long 2006 Adaptive Sampling and Prediction (ASAP) field experiment in Monterey Bay, California. One of the central goals of the field experiment was to test and demonstrate newly developed techniques for coordinated motion control of autonomous vehicles carrying environmental sensors to efficiently sample the ocean. We describe the field results for the heterogeneous fleet of autonomous underwater gliders that collected data continuously throughout the month-long experiment. Six of these gliders were coordinated autonomously for 24 days straight using feedback laws that scale with the number of vehicles. These feedback laws were systematically computed using recently developed methodology to produce desired collective motion patterns, tuned to the spatial and temporal scales in the sampled fields for the purpose of reducing statistical uncertainty in field estimates. The implementation was designed to allow for adaptation of coordinated sampling patterns using human-in-the-loop decision making, guided by optimization and prediction tools. The results demonstrate an innovative tool for ocean sampling and provide a proof of concept for an important field robotics endeavor that integrates coordinated motion control with adaptive sampling.

1. INTRODUCTION

The recent proliferation of autonomous vehicles and advanced sensing technologies has unleashed a pressing demand for the design of adaptive and sustainable observational systems for improved understanding of natural dynamics and human-influenced changes in the environment. A central problem is designing motion planning and control for networks of sensor-equipped, autonomous vehicles that yield efficient collection of information-rich data. The coastal ocean presents an unusually compelling yet challenging context for advanced observational systems. Because of the distinct dearth of data on both physical and biological phenomena below the ocean surface, understanding of coastal ocean and ecosystem dynamics remains critically incomplete. Approaches to the collection of revealing data must address the significant challenges of motion control, sensing, navigation, and communication in the inhospitable, uncertain, and dynamic ocean.

In this paper we present the experiment design and results of the coordinated control of a fleet of 10 autonomous underwater gliders (of two varieties) carried out in Monterey Bay, California, during the August 2006 field experiment of the Adaptive Sampling and Prediction (ASAP) research initiative. The ASAP 2006 field experiment in Monterey Bay demonstrated and tested an adaptive coastal ocean observing system featuring the glider fleet as an autonomous, mobile sampling network. The ASAP system combined the autonomous and adaptively controlled sampling vehicles with real-time, data-assimilating dynamical ocean models to observe and predict conditions in a 22 × 40 km and up to more than 1,000-m-deep region of coastal ocean just northwest of Monterey Bay [see Figure 1(a)]. The system ran successfully over the course of the entire month of August 2006, with the gliders sampling continuously and coordinating their motion to maximize information in the data collected, in spite of strong, variable currents and changing numbers of available gliders. The motion of six of the gliders was autonomously coordinated for 24 days straight.

The glider network tested in the 2006 ASAP field experiment is distinguished by its autonomous, coordinated, and sustained operation and its responsiveness to the demands of the adaptive ocean sampling mission and the dynamic state of the ocean. Accordingly, the field results demonstrate a new capability for ocean sampling and further suggest promising opportunities for application to collaborative robotic sensing in other domains. Notably, the ASAP experiment provides a proof of concept in the field for the methodology, defined and justified in Leonard, Paley, Lekien, Sepulchre, Fratantoni, et al. (2007), that integrates coordinated motion control with adaptive sampling. This methodology decouples, to advantage, the design of coordinated patterns for high-performance sampling from the design of feedback control laws that automatically drive vehicles to the desired coordinated patterns.

The coordinating feedback laws for the individual vehicles derive systematically from a control methodology (Sepulchre, Paley, & Leonard, 2007, 2008) that provides provable convergence to a parameterized family of collective motion patterns. These patterns consist of vehicles moving on a finite set of closed curves with intervehicle spacing prescribed by a small number of "synchrony" parameters. The feedback laws for the individuals that stabilize a given pattern are defined as a function of the same synchrony parameters that distinguish the desired pattern. Significantly, these feedback laws do not require a prescription of where each vehicle should be as a function of time; instead they are reactive: each vehicle moves in response to

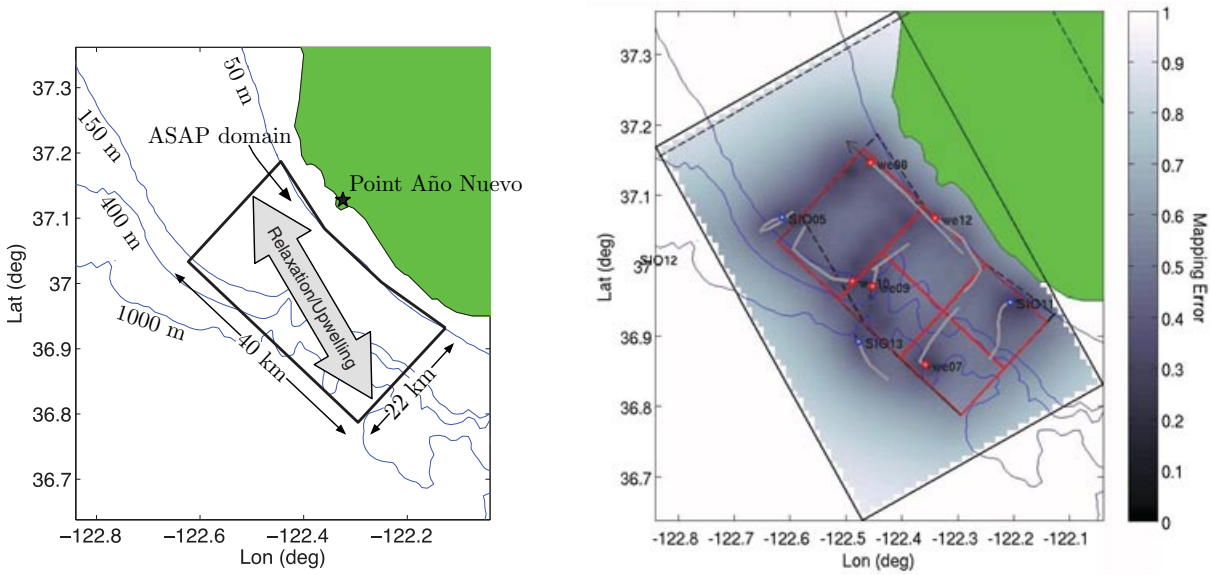

Figure 1. (a) Region of glider fleet operations in the 2006 ASAP field experiment, just northwest of Monterey Bay, California. The summertime ocean circulation in Monterey Bay oscillates between upwelling and relaxation. During an upwelling event, cold water often emerges just north of the bay, near Point Año Nuevo, and tends to flow southward across the mouth of the bay. During relaxation, poleward flows crosses the mouth of the bay past Point Año Nuevo. (b) Objective analysis mapping error (see Section 2.2) plotted in gray scale on the ASAP sampling domain for July 30, 2006, at 23:30 GMT. Eight gliders are shown; their positions are indicated with circles.

the relative position and direction of its neighbors so that as it keeps moving, it maintains the desired spacing and stays close to its assigned curve. For example, it has been observed in the field that when a vehicle on a curve is slowed down by a strong opposing flow field, it will cut inside a curve to make up distance and its neighbor on the same curve will cut outside the curve so that it does not overtake the slower vehicle and compromise the desired spacing. There are no leaders in the network, which makes the approach robust to vehicle failure. The control methodology is also scalable because the responsive behavior of each individual can be defined as a function of the state of a small number of other vehicles, independent of the total number of vehicles. Implementation in the field is made possible by means of the Glider Coordinated Control System (GCCS) software infrastructure described by Paley, Zhang, and Leonard (2008) and tested by Zhang, Fratantoni, Paley, Lund, and Leonard (2007). The field experiment results described here successfully demonstrate this methodology in the challenging coastal ocean environment.

As discussed in Leonard et al. (2007), the decoupling in the overall methodology is advantageous because it allows for the design of collective motion patterns, independent of individual vehicle feedback laws, to (1) optimize a sampling performance metric, (2) reduce performance sensitivity to disturbances in vehicle motion, and (3) take into account design requirements and constraints, such as ensuring direct coverage (or avoidance) of certain regions, leveraging information on the direction of strong currents (to move with rather than against them) and accommodating a changing number of available vehicles. The methodology also makes possible human-in-the-loop supervisory control when it is desirable; this can be critical for highly complex experiments. In the ASAP experiment, a team of scientists collaborated to make supervisory decisions given information on observed and predicted ocean dynamics, system performance, and vehicle availability. These decisions were translated into adaptations of the desired collective motion patterns, which were refined using numerical optimization tools. The adaptations were implemented as intermittent, discrete changes in the patterns to which the vehicle network responded automatically. The field experiment results demonstrate the capability for adaptation of patterns and the integration of human decision making in a complex multirobot sensing task.

The ASAP effort builds on experience from the 2003 Autonomous Ocean Sampling Network II (AOSN-II) month-long field experiment in Monterey Bay (Haddock & Fratantoni, 2009; Ramp, Davis, Leonard, Shulman, Chao, et al., 2009) in which a network of data-gathering vehicles, featuring a fleet of gliders, was integrated with advanced real-time ocean models. In two multiday sea trials run during the 2003 experiment, three gliders were coordinated with automated feedback control to move in triangular formations, to estimate gradients from scalar measurements, and to investigate the potential for adaptive gradient climbing in a sampled field (Fiorelli, Leonard, Bhatta, Paley, Bachmayer, et al., 2006). In a third daylong sea trial, a glider used feedback control to follow a Lagrangian drifter in real time and to demonstrate the potential of a glider (or gliders) to track Lagrangian features such as a water mass encompassing an algal bloom (Fiorelli et al., 2006). For the remainder of the AOSN-II experiment, gliders were operated without coordinated control on linear and trapezoidal tracks in a region extending as far as 100 km from shore. In Leonard et al. (2007), sampling performance (as measured by information in data collected) was evaluated for the gliders on their tracks: when the currents were strong, the gliders were pushed together and performance deteriorated. This motivated the investigation of active coordinated control of gliders to improve sampling performance (Leonard et al., 2007) that led to the glider control implementation in the ASAP experiment.

The AOSN-II and ASAP field experiments were inspired by earlier experiments with ocean observing and prediction systems; see, for example, Bogden (2001), Dickey (2003), Robinson and Glenn (1999), and Schofield, Bergmann, Bissett, Grassle, Haidvogel, et al. (2002). Other relevant experiments making use of multiple underwater vehicles include, for example, the experiments described by Bellingham and Zhang (2005), Chappell, Komerska, Blidberg, Duarte, Martel, et al. (2007), Glenn, Jones, Twardowski, Bowers, Kerfoot, et al. (2008), Maczka and Stilwell (2007), Schulz, Hobson, Kemp, and Meyer (2003), and Smith, Chao, Li, Caron, Jones, et al. (2010). Sampling strategies designed to minimize uncertainty in ocean model predictions using advanced ocean modeling techniques include those of Bishop, Etherton, and Majumdar (2001), Lermusiaux (1999), Lermusiaux and Robinson (1999), Majumdar, Bishop, and Etherton (2002), and Shulman, McGillicuddy, Moline, Haddock, Kindle, et al. (2005). Other relevant work pertains to adaptive sampling (Rahimi, Pon, Kaiser, Sukhatme, Estrin, et al., 2004; Jakuba & Yoerger, 2008), optimization of survey strategies (Richards, Bellingham, Tillerson, & How, 2002; Willcox, Bellingham, Zhang, & Baggeroer, 2001), and flux computations using underwater measurements (Thomson, Mihaly, Rabinovich, McDuff, Veirs, et al., 2003; Zhong & Li, 2006). The field experiment described in this paper represents the single largest (10 vehicles) and longest (24 days) deployment of coordinated, underwater robotic vehicles that we are aware of.

In Section 2 we review underwater gliders and the sampling performance metric of Leonard et al. (2007) and summarize the 2006 ASAP field experiment in Monterey Bay. We describe the plan to control and coordinate the fleet of autonomous underwater gliders in Section 3. Results of the glider network operation during the field experiment are provided in Section 4. Some of the results were first reported in Paley (2007). We examine the

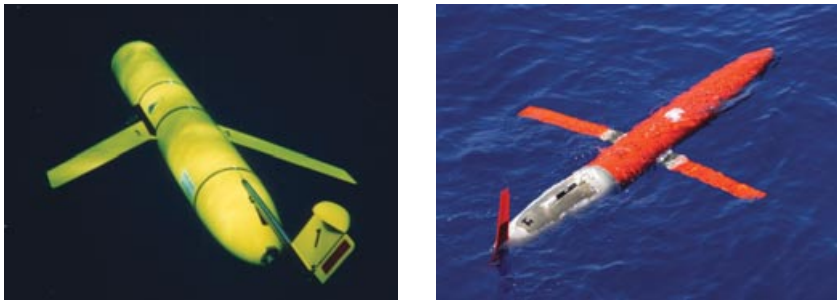

(a) Slocum glider (b) Spray glider

Figure 2. Slocum and Spray gliders used in the 2006 ASAP experiment.

performance of the gliders in Section 5 and make final remarks in Section 6.

2. BACKGROUND AND MOTIVATION

We begin in Section 2.1 with a description of the underwater gliders that make up the mobile sensor network featured in the 2006 ASAP field experiment. In Section 2.2 we review the sampling performance metric that is central to the coordinated control and adaptive sampling methodology defined and justified in Leonard et al. (2007) and demonstrated in the ASAP field experiment. Section 2.3 follows with a summary of the motivation, context, and highlights of the ASAP field experiment.

2.1. Autonomous Underwater Gliders

Gliders are buoyancy-driven autonomous underwater vehicles optimized for endurance; they can operate continuously for weeks to months by maintaining low speeds and low drag and limiting energy consumption with low-power instrumentation. Generally slower than propeller-driven vehicles, gliders propel themselves by alternately increasing and decreasing their buoyancy using either a hydraulic or a mechanical buoyancy engine. Lift generated by flow over fixed wings converts the vertical ascent/descent induced by the change in buoyancy into forward motion, resulting in a sawtooth-like trajectory.

A heterogeneous fleet of gliders was selected to provide a range of capabilities suited to the ocean depths in the ASAP operating region [Figure 1(a)]. Four Spray gliders (Rudnick, Davis, Eriksen, Fratantoni, & Perry, 2004; Sherman, Davis, Owens, & Valdes, 2001) manufactured by Bluefin Robotics/Teledyne are rated to 1,500-m depth and were operated by the Scripps Institution of Oceanography (SIO). Six Slocum gliders (Webb, Simonetti, & Jones, 2001) manufactured by Teledyne Webb Research Corp. are rated to 200-m depth and were operated by the Woods Hole Oceanographic Institution (WHOI). Both glider variants are approximately 2 m in length and weigh 50 kg in air (Figure 2). The gliders steer in the horizontal plane either by moving an internal mass to bank and turn (Spray) or by deflecting an external rudder (Slocum). Both vehicles use iridium satellite telephones to communicate bidirectionally with a shore station.

Ocean currents substantially impact the navigation of a slow vehicle. Glider speed relative to the surrounding water is generally 0.3–0.5 m/s in the horizontal direction and 0.2 m/s in the vertical. Underwater deduced reckoning using measurements of vehicle pitch and ascent/descent rate results in positional inaccuracies of 10%–20% of distance traveled. Vehicle position is corrected when the vehicle returns to the surface and acquires a global positioning system (GPS) fix. Differences between the estimated surface position and a satellite fix can be interpreted as a time/space/depth average of the ocean velocity (i.e., set and drift).

Gliders carry sensors to measure the underwater environment. All vehicles were equipped with conductivity–temperature–depth (CTD) sensors to measure temperature, salinity, and density and chlorophyll fluorometers to estimate phytoplankton abundance. The four Spray gliders—SIO05, SIO11, SIO12, SIO13—also carried Sontek 750-kHz acoustic Doppler profilers (ADPs) to measure variations in water velocity and acoustic backscatter. The six Slocum gliders—we05, we07, we08, we09, we11, and we12—carried additional optical backscatter and light sensors.

The set of all measurements of a single scalar signal collected during a glider descent or ascent is termed a *profile*. A profile is associated with a single horizontal position that corresponds to the glider position at either the start or the end of the dive. Thus, a profile provides a sequence of measurements, with each measurement corresponding to a different depth but the same horizontal position. At each surfacing each glider transmitted profile data, position and status information, and an updated estimate of ocean current via satellite telephone. Each glider was also able to receive updated instructions from the shore station at each surfacing.

2.2. ASAP Ocean Sampling Metric

The glider network was deployed in the ASAP experiment to test the ability to carry out, in the challenging coastal ocean environment, the coordinated control and adaptive sampling methodology presented in Leonard et al. (2007). A sampling performance metric is defined and justified in Leonard et al. (2007), and a parameterized set of coordinated motion patterns is examined with respect to this metric. The design methodology provides a systematic prescription of feedback control laws that coordinate vehicles onto motion patterns designed to optimize the sampling performance metric. The sampling metric was computed in real time during the ASAP experiment so that performance could be evaluated as part of human decision making for adaptations. The sampling metric is examined in this paper as a means to identify ocean conditions and operating conditions during the experiment that reduced sampling performance and to examine control and adaptation solutions that improved sampling performance.

The sampling metric, defined in Leonard et al. (2007), derives from the residual uncertainty (as measured by mapping error) of the data assimilation scheme known as *objective analysis* (OA) (Bretherton, Davis, & Fandry, 1976; Gandin, 1965), which provides a linear statistical estimation of a sampled field. Because reduced uncertainty, equivalent to increased entropic information, implies better measurement coverage, the OA mapping error, or the corresponding information, can be used as a sampling performance metric. The *mapping error* at position R and time t is the error variance $\hat{C}(R, t, R, t)$. The error variance depends on where and when data are taken and on an empirically derived model of the covariance of fluctuations of the sampled field about its mean. For the ASAP experiment the covariance of fluctuations $C(R, t, R', t')$ is assumed to be $\sigma_0 e^{-\Gamma(R,R')/\sigma - |t-t'|/\tau}$, where $\sigma_0 = 1$, $\sigma = 22$ km is the spatial decorrelation length, and $\tau = 2.2$ days the temporal decorrelation length, all based on estimates from previous glider data (Rudnick et al., 2004). $\Gamma(R, R')$ is a measure of the distance between R and R' on the Earth (Paley, 2007). A snapshot of the OA mapping error from the 2006 ASAP experiment is shown in Figure 1(b).

Following Leonard et al. (2007), the *mapping error in mapping domain* $\mathcal{B}$ is defined as

$$\mathcal{E}(t) = \frac{1}{\sigma_0 |\mathcal{B}|} \int_{\mathcal{B}} \hat{C}(R, t, R, t) dR, \tag{1}$$

where $|\mathcal{B}|$ is the area of $\mathcal{B}$. Likewise the *mapping error on the boundary* $\delta\mathcal{B}$ *of* $\mathcal{B}$ denoted $\mathcal{E}_\delta(t)$ is defined as in Eq. (1) with $\delta\mathcal{B}$ replacing $\mathcal{B}$ everywhere. The *sampling performance metric* is defined as $\mathcal{I}(t) = -\log \mathcal{E}(t)$, which describes the amount of information at time t contained in the measurements (Grocholsky, 2002). The metric $\mathcal{I}_\delta(t) = -\log \mathcal{E}_\delta(t)$ defines the amount of information at time t on the boundary.

2.3. ASAP Experiment

The long-term goal of the ASAP research initiative is "to learn how to deploy, direct and utilize autonomous vehicles and other mobile sensing platforms most efficiently to sample the ocean, assimilate the data into numerical models in real or near-real time and predict future conditions with minimal error" (Leonard, Ramp, Davis, Fratantoni, Lermusiaux, et al., 2006). Toward this goal, the 2006 ASAP field experiment was designed to demonstrate the integration of new techniques in sensing, forecasting, and coordinated control. The oceanographic context was the three-dimensional dynamics of the coastal upwelling center in Monterey Bay and the processes governing the heat budget of the 22 × 40 km control volume during periods of upwelling-favorable winds and wind relaxations. A scientific study, based on data and model output, of the oceanographic and atmospheric conditions during the ASAP experiment is described by Ramp, Lermusiaux, Shulman, Chao, Wolf, et al. (2010). In the present paper we describe a central part of the ASAP experiment: the demonstration of new methodology for automated coordinated control of the glider fleet for adaptive ocean sampling.

Strategies for the coordinated glider sampling were planned to be responsive to the dynamics of intermittent upwelling events in Monterey Bay. The summertime ocean circulation in Monterey Bay is primarily controlled by variability in alongshore wind forcing (Rosenfeld, Schwing, Garfield, & Tracy, 1994). During periods of strong equatorward winds, surface water is advected offshore, leading to nearshore upwelling of cold, nutrient-rich subsurface water, which can spur primary productivity (i.e., enhanced growth of phytoplankton) in the vicinity of the bay (Olivieri & Chavez, 2000; Suzuki, Preston, Chavez, & DeLong, 2001). This productivity, combined with the ocean circulation, results in complex dynamics of carbon production and advection (Pilskaln, Paduan, Chavez, Anderson, & Berelson, 1996). Cold upwelled water often emerges just north of the bay, near Point Año Nuevo [see Figure 1(a)] and flows southward across the mouth of the bay. During periods of active upwelling, the water temperature in the bay can be elevated, a phenomenon known as "shadowing" (Graham & Largier, 1997) Periods of weaker, poleward winds (termed "relaxation") result in northward near-surface flow across the mouth of the bay and alongshore near Point Año Nuevo. Transitions between states can produce complex scenarios in which both poleward and equatorward flows are observed simultaneously. In certain instances, onshore flow bifurcates (divides into two branches) near Point Año Nuevo. The summertime ocean circulation oscillates between upwelling and relaxation states but is also influenced by several year-round components of the California Current System (CCS) (Ramp et al., 2009), e.g., the California undercurrent—a deep, poleward flow (Ramp, Paduan, Shulman, Kindle, Bahr, et al., 2005).

During the experiment, data were collected also from a Naval Postgraduate School research aircraft, satellite imagery, and high-frequency radar. Data were available outside the control volume from several moorings, drifters deployed by the Monterey Bay Aquarium Research Institute (MBARI), and other ships and vehicles. Data were assimilated regularly into three different high-resolution ocean models: the Harvard Ocean Prediction System (HOPS) (Robinson, 1999), the Jet Propulsion Laboratory implementation of the Regional Oceanic Modeling System (JPL/ROMS) (Shchepetkin & McWilliams, 2004), and the Navy Coastal Ocean Model/Innovative Coastal Ocean Observing Network (NCOM/ICON) (Shulman, Wu, Lewis, Paduan, Rosenfeld, et al., 2002), each of which produced daily updated ocean predictions of temperature, salinity, and velocity. All observational data and model outputs were made available in near-real time on a central data server at MBARI. A virtual control room (VCR), also running off the MBARI server, was developed for the 2006 ASAP field experiment so that all participants could remain at their distributed home institutions throughout the experiment but still be fully informed and connected with the team (Godin, Bellingham, Rajan, Leonard, & Chao, 2006); panels on the VCR allowed for team decision making and voting.

Prior to the field experiment, the coordinated control and adaptive sampling were rehearsed during five virtual pilot experiments; these were run just like the real field experiments except that the hardware was replaced with simulated vehicles moving in the currents of a virtual ocean defined by a HOPS reanalysis of Monterey Bay in 2003. The GCCS was used in simulation mode to simulate and control the gliders, implementing communication paths and data flow identical to those used in the 2006 field experiment (Paley, 2007; Paley et al., 2008).

3. PLAN AND APPROACH TO OPERATIONS FOR GLIDER FLEET

3.1. Glider Plan Overview

The plan for operating the glider fleet during the 2006 ASAP field experiment was driven by requirements for the data collected, by an interest in leveraging the opportunity to coordinate the motion of the gliders to maximize value in the data collected, and by the need for adaptability of the sampling strategy to changes in the ocean, changes in mapping uncertainty, changes and constraints in operations, and unanticipated challenges to sampling such as strong currents. Because the methodology for coordinated control and adaptive sampling as described and argued by Leonard et al. (2007) is well suited to address these requirements, it was adopted for the gliders in the ASAP field experiment.

The experiment's ocean science objective was defining and measuring the key components of the coastal-upwelling heat budget. Conceptually this involves measuring changes throughout the interior of the control volume as well as fluxes acting through the periphery of that volume. Both the sensor and sampling requirements for these two measurement types differ. For the interior, measurements of properties such as water temperature, density, and in-water radiation made throughout the control volume are primary. To close mass and heat budgets, we require knowledge of horizontal fluxes along the control volume's lateral boundaries. Horizontal mass fluxes are determined from measured velocities, whereas heat fluxes depend on both measured velocity and temperature. The large-scale, low-frequency component of the oceanic velocity field (the geostrophic flow: a balance between lateral pressure gradients and accelerations due to the Earth's rotation) is determined indirectly from a three-dimensional density field constructed from direct measurements of temperature, salinity, and pressure. Smaller scale or time-dependent aspects of the circulation (ageostrophic flows, such as those resulting from frictional boundary processes) cannot be inferred from the density field and must be explicitly measured. The control volume bottom is the seafloor or 500-m depth through which transport is assumed to be small.

The differing interior and peripheral sampling requirements were assigned to the two different kinds of gliders. The plan was to have the Slocum gliders map the interior volume by coordinated sampling on closed curves and relying on interpolation to infer properties between measured paths. The Spray gliders were to maintain distributed sampling along the periphery by having each glider patrol a segment of the boundary in an oscillatory manner. Sprays were chosen for this role because they dive deeper and carry ADPs to directly measure velocity, which is needed in ageostrophic boundary layers at the surface and bottom.

The methodology Leonard et al. (2007) used for coordinated control and adaptive sampling separates the design of coordinated patterns for high-performance sampling from the design of feedback control laws that coordinate the motion of vehicles to the desired patterns. The plan was to start the experiment with a default coordinated motion pattern (shown in Figure 3) and then to redesign and update the coordinated motion pattern as warranted to address changing environmental and operating conditions. The feedback laws to automatically coordinate the Slocum gliders to the selected motion pattern were implemented using the GCCS.

Following Leonard et al. (2007), the motion patterns were designed to coordinate the gliders to move around a finite set of curves, with intervehicle spacing prescribed for gliders on the same curve and spatial synchronization prescribed for gliders on different curves. The curves for Slocums were closed and selected among those with nearly straight long sides and orientation such that the gliders would cross over the shelf break (the end of the continental shelf characterized by a sharp increase in the slope of the

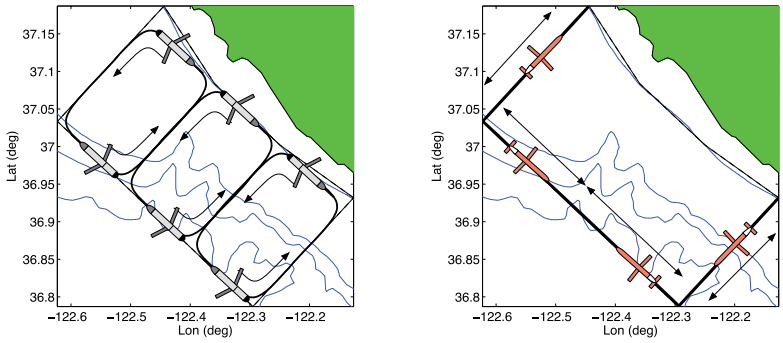

(a) Slocum gliders (b) Spray gliders

Figure 3. Initial default motion pattern for the 10 gliders in the 2006 ASAP field experiment.

ocean bottom). Each time a glider would travel around a curve, it would sample a cross section of the dynamic ocean processes that propagate parallel to the shelf break. By constructing a time sequence of cross-section plots, it would then be possible to reconstruct, identify, and monitor ocean processes even before assimilating the glider profile data into an advanced ocean model. The curves for Sprays were segments of the control volume periphery where boundary fluxes were measured as part of mass and heat budgets.

The dimensions and locations of the curves and, importantly, how the gliders were distributed relative to one another around the curves were selected to maximize the sampling performance metrics $\mathcal{I}(t)$ and $\mathcal{I}_\delta(t)$. For example, in the initial default motion pattern for the six Slocum gliders, shown in Figure 3(a), there are three superelliptical curves (tracks) (Paley, 2007) and two gliders assigned to each track. Each pair of gliders on a given track should move at the common (maximum) speed, keeping maximal track distance between them, whereas the three glider pairs should synchronize across tracks, as shown in the figure. The default direction of travel was chosen with an interest in having gliders move in the same direction as the strongest currents, anticipated to be offshore in the direction of the equator.

In accordance with the different assignments for the Slocum and Spray gliders, the method of control and coordination used for the Slocum gliders was different from the approach used for the Spray gliders. Automated control was demonstrated in both cases as it is an important ingredient for sustainability and optimal performance of ocean observing systems. The differences derived from alternative approaches to addressing strong currents; for gliders, control in a varying current field is inexact and control in currents that are faster than the glider's forward speed is impossible.

In the case of the Slocum gliders, adaptations in the defining coordinated motion pattern could be made with human input to address the strongest currents. For example, the direction of glider motion around tracks would be reversed in the event that adverse currents were impeding the motion of the gliders. As a result, control of the gliders to the desired pattern could be completely automated because the feedback would need to counter only weaker currents. Automated coordinated feedback control of Slocum gliders operated continuously with motion patterns updated as momentary interruptions. In the case of the Spray gliders, on the other hand, there was not much flexibility in adapting the pattern to address adverse currents because the overall plan required the Sprays to be on the boundary. The important control on the boundary was the time/position at which each glider reversed its direction of travel to increase sampling performance on the boundary; these course reversals could be adaptively adjusted with human input. Sprays would then use various automated steering modes to approach waypoints, maintain a heading, steer relative to the current velocity, or direct a glider back toward its intended path while proceeding to a waypoint; see Leonard et al. (2006).

The plan for the operation of the gliders made significant use of new automated control methodology while deliberately making possible the smooth integration of intermittent decision making from a human team. Figure 4 illustrates some key components, data flow and program flow in the coordinated control of Slocum and Spray gliders as implemented in the 2006 ASAP experiment. For details of data flow associated with the GCCS, see Figure 3 of Paley et al. (2008). Below we summarize the approach to the operation of both Spray and Slocum gliders.

3.2. Approach to Operation of Slocum Gliders

The Slocum gliders were autonomously controlled to a prescribed coordinated motion pattern that could be adapted as desired. The prescription of motion patterns and a computational tool for optimizing patterns with respect to the sampling performance metric are reviewed in Section 3.2.1.

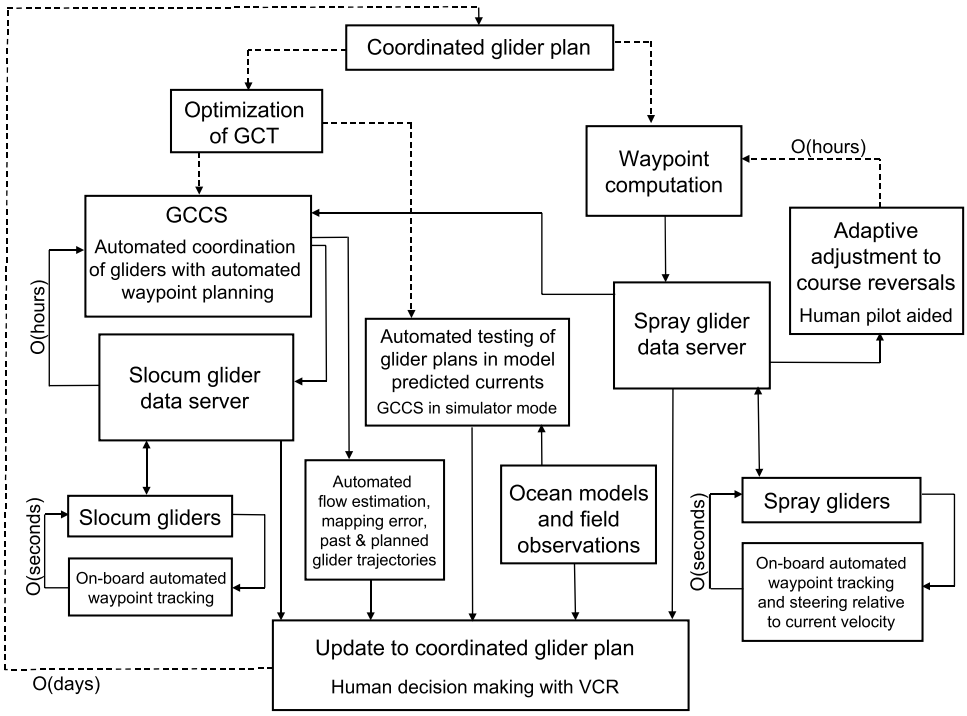

Figure 4. Overview of some key components (blocks), data flow (solid arrows), and program flow (dashed arrows) in the coordinated control of Slocum and Spray gliders as implemented during the 2006 ASAP experiment. Not shown, for example, is the flow of measurement data from the Slocum and Spray data servers to the ocean models. The labels on the feedback loops indicate the order of magnitude of the feedback sampling period. GCCS refers to the Glider Coordinated Control System. GCT refers to the set of glider coordinated trajectories that define the coordinated motion pattern. VCR refers to the virtual control room.

Adaptation of motion patterns was expected to occur on the order of every 2 days. The prescribed motion pattern was an input to the GCCS software infrastructure that automated the coordinated control of the Slocum gliders. The GCCS, reviewed in Section 3.2.2, ran on a computer at Princeton University throughout the experiment, communicating with the gliders through a server at WHOI. Each Slocum glider communicated with the WHOI server when it surfaced, approximately every 3 h, but gliders were not synchronized to surface at the same time. Although the coordinating control law was run on a single computer, it used a decentralized control law, i.e., the reactive behavior computed for each individual vehicle was defined as a function of the relative state of a subset of the other gliders. The Slocum gliders automatically carried out the coordinated control directives using their own onboard feedback laws. The GCCS is described comprehensively by Paley et al. (2008), and details of its implementation in the ASAP field experiment are presented by Paley (2007).

The pattern adaptation decisions were made by humans with the aid of computational tools, including the optimization tool described below, continuous computations of the sampling performance metric, ocean currents from glider estimates as well as advanced ocean model forecasts, situational awareness updates, and discussion and voting panels all made available on the VCR. Additionally, in parallel with GCCS implementation for the field operations, the GCCS was used to preview coordinated glider motion plans in faster than real time with simulations in ocean model–predicted currents, described further in Section 3.2.3.

The advantage of the GCCS architecture is its easy adoption, versatility (e.g., in integrating automation with humans in the loop when appropriate), and wide applicability (with respect to different types of gliders) as opposed to a completely onboard, decentralized approach, which would require substantial sea trials to test and validate specialized software and could severely constrain coordinated sampling because of limited available means for glider-to-glider sensing over a large sampling domain. The disadvantage is that the GCCS implements decentralized control algorithms in a centralized manner, which requires regular communication between the gliders and the shore station.

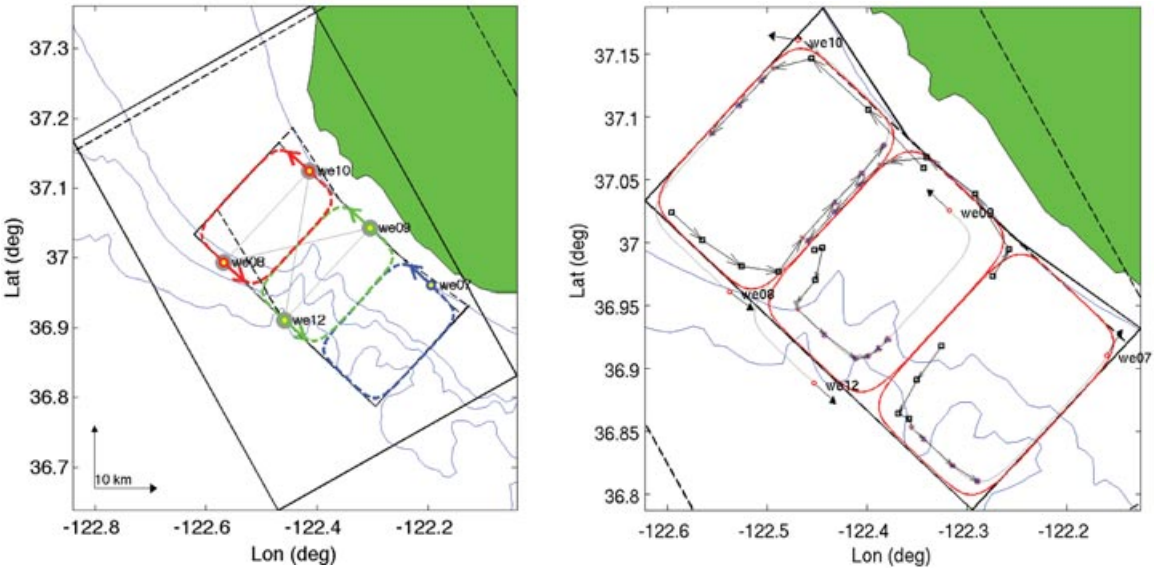

(a) GCT 2

(b) GCCS planner panel, July 30, 2006, at 23:10 GMT

Figure 5. (a) GCT 2 defines a coordinated pattern for the four Slocum gliders, with the pair we08 and we10 to move on opposites of the north track, the pair we09 and we12 on opposites of the middle track, and the two pairs synchronized on their respective tracks. Glider we07 should move independently around the south track (the sixth glider had not yet been deployed). The dashed lines show the superelliptical tracks, the circles show a snapshot of the glider positions, and the color coding defines each glider's track assignment. The thin gray lines show the feedback interconnection topology for coordination (all but we07 respond to each other), and the arrows show the prescribed direction of rotation for the gliders. (b) Several real-time status and assessment figures, movies, and logs were updated regularly on the Glider Planner and Status page (Princeton University, 2006a). Shown here is a snapshot of one of the panels, which was updated every minute. It presents, for each glider, surfacings over the previous 12 h (squares), waypoints expected to be reached before the next surfacing (gray triangle), next predicted surfacing (gray circle with red fill), new waypoints over the next 6 h (blue triangles), and planned position in 24 h (hollow red circle). Each glider is identified with a label at the planned position in 24 h.

3.2.1. Design and Local Optimization of GCTs

A desired motion pattern for the fleet of gliders under GCCS control is specified as a set of *glider coordinated trajectories* (GCT). A GCT has three main components, all contained in an XML file and used as input to the GCCS (Princeton University, 2006c). The first component is the operating domain, which specifies the shape, location, size, and orientation of the region where the gliders operate. The second component is the track list, which specifies the name, shape, location, size, orientation, and other properties of the closed loops (tracks) around which the gliders should travel. The third component is the glider list, which specifies the glider properties including track assignments, interaction network for coordinating control (which glider is responding to which other glider in the feedback laws), and desired steady-state pattern of the gliders on their tracks (including relative spacing on tracks and synchronization across tracks). The GCT file can be converted into a picture; see, for example, Figure 5(a), which shows GCT 2 on July 30 when the first five Slocum gliders deployed were carrying out the default pattern of Figure 3(a).

Adaptations to sampling plans were implemented by switching to a new GCT. In the case of a switch of GCT, the GCCS would be manually interrupted, the new GCT file swapped for the old one, and then the GCCS restarted. The Princeton Glider Planner and Status page (Princeton University, 2006a), linked to the VCR, was consulted for determining adaptations as it maintained up-to-date maps of glider positions and GCCS planning, OA predicted currents over the region based on the 10 gliders' own depth-averaged current estimates, and OA mapping error and sampling performance. Figure 5(b) shows a snapshot of the glider planner status panel on July 30 at 23:10 GMT (Greenwich Mean Time) when the GCCS was controlling the gliders to GCT 2. Figure 1(b) shows a corresponding snapshot of the glider planner panel for OA mapping error on July 30 at 23:30 GMT.

Any pattern under consideration for use as a GCT could be locally optimized using the online interactive Princeton Glider Optimization Page (Princeton University, 2006c). The automated optimization of GCTs consists of modifying some of the parameters in order to maximize the

sampling performance metric. Consider, for example, the GCT 2 configuration depicted in Figure 5(a). This contains information that should not be modified, such as the track distribution, the assignment of specific gliders to the three tracks, and the linkage between pairs of gliders on the same track, as well as the coupling between the motion on the three tracks. During the experiment, we considered the relative positioning between the individual gliders as tunable parameters.

Optimizing the sampling metric consists of minimizing the time average of the mapping error $\mathcal{E}(t)$. The ability to optimize the GCT in real time depends on our ability to evaluate the metric sufficiently fast for arbitrary configurations. This objective was achieved by thresholding the correlation matrix (terms below 10^{-4} are set to zero), solving the time integral analytically, and using piecewise linear interpolation on a mesh of triangles for the spatial integrals (see Figure 6). We then used a combination of gradient climbing and random walk in parameter space to optimize the GCT.

The optimizer was linked to the web page (Princeton University, 2006c), where input GCT files could be uploaded and plotted. Upon submission, the engine would continuously optimize the GCT until a new input file was loaded. At any time, the web page displayed the best GCT found so far and the output could be used to replace the active GCT in the GCCS by the optimized version.

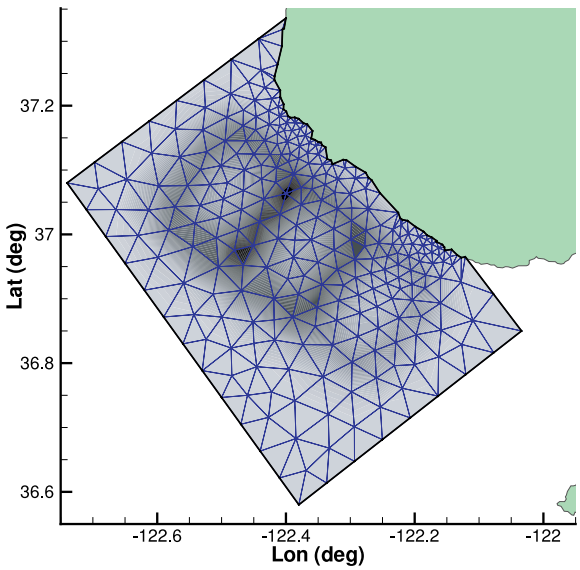

Figure 6. Mesh of triangles used to approximate the integral in the computation of the ASAP sampling performance metric is superimposed on the computed error map for optimization of GCT 2 (shown in Figure 5). The south track is lighter (lower performance) because there is only one glider on it. The darkest line is the common edge of the two upper tracks as four gliders travel on it.

3.2.2. Coordinated Control and the GCCS

The GCCS is a modular, cross-platform software suite written in MATLAB (Paley et al., 2008). The three main modules are (i) the planner, which is the real-time controller; (ii) the simulator, which can serve as a control test bed or for glider motion prediction; and (iii) the remote input/output module, which interfaces to gliders indirectly through the glider data servers. To plan trajectories for the gliders, which surface asynchronously, the GCCS uses two different models: a simple glider model (called the particle integrator), with gliders represented as particles, that is integrated to plan desired trajectories with coordinated control, and a detailed glider model (called the glider integrator) that is integrated to predict three-dimensional glider motions in the presence of currents.

The GCCS planning process is described by Paley et al. (2008) and summarized here. The planned trajectories originate from the position and time of the next expected surfacing of each glider. Planning new trajectories for all gliders occurs simultaneously; the sequence of steps that produces new glider trajectories is called a planning cycle. A planning cycle starts whenever a glider surfaces and ends when the planner generates new waypoints for all gliders. The planner uses the detailed glider model to predict each glider's underwater trajectory and next surfacing location and time. This prediction uses the surface and underwater flow OA forecast obtained from all recent glider depth-averaged current estimates. For each glider that has surfaced since the last planning cycle, the planner calculates inaccuracies in the predictions of effective speed, expected surface position, and expected surface time. Effective speed decreases with time spent on the surface; it is computed as the horizontal distance between sequential profile positions divided by the time interval between the profile times. Prediction errors are useful for gauging glider and planner performance.

The coordinated control law used in the particle integrator is a decentralized control algorithm that steers self-propelled particles onto symmetric patterns defined by the GCT. Each particle steers in response to measurements of relative headings and relative positions of neighbors, i.e., the feedback laws are reactive. Neighborhoods are defined by the interconnection topology prescribed in the GCT (shown as thin gray lines in the GCT pictures). The coordinating feedback laws for the individual vehicles derive systematically from a control methodology (Sepulchre et al., 2007, 2008) that provides provable convergence to the desired pattern. The precise control law used in the ASAP field experiment is defined in Paley (2007).

3.2.3. Testing Plans in Model Predicted Currents

In parallel with the GCCS controlling the real gliders, three additional copies of the GCCS performed virtual experiments on a daily basis using the forecasts from the three ocean models HOPS, JPL/ROMS, and NCON/ICON. Each ocean model generated forecasts from a starting time at regular intervals on the order of every 6 h to at least 24 h into the future (48- and 72-h forecasts were also provided). Thus, faster-than-real-time simulations of gliders moving in the forecast ocean provided predictions of how the gliders would perform in the real ocean. All four copies of the GCCS implemented identical autonomous control laws, and the initial positions of the simulated gliders were set to be identical to the (best estimate) positions of the gliders in the ocean.

Each virtual experiment ran from between 2 and 5 h, depending on how far into the future the simulation was computed. The simulation results were organized and reported online at the Princeton Glider Prediction Page (Princeton University, 2006b). In addition to providing the daily predictions, the glider prediction tool was available for use on demand.

After the predicted period of time had passed (e.g., the next day if the predicted period was 24 h), the trajectories of the real gliders in the ocean were compared with prediction results. The prediction error measures flow prediction error together with modeling errors in the glider simulator. It has the potential to be used as a feedback to the models and as a means to determine the certainty with which the predictions can be used to influence adaptation decisions.

3.3. Approach to Operation of Spray Gliders

Because only Sprays carried ADPs to directly measure the velocity critical to observing boundary fluxes, their array was optimized independently of the Slocums. Fluxes through the land were neglected, and only the offshore and two cross-shelf edges of the control volume were considered. Mission planning and adaptation were formally structured as for the Slocum gliders, but because the objective was sampling performance on a line, the two-step control optimization scheme was simplified greatly. The ideal path (the control-volume boundary) was divided into four equal-length segments (two cross-shelf sectors and the two halves of the offshore line) with each glider oscillating back and forth in its sector, ideally maintaining equal along-track separation from its neighbors. This synchronization is feasible only if currents are weak. Experimentation with the mapping error $\mathcal{E}_\delta(t)$ showed little degradation of integrated mapping error so long as pairs of gliders were not within $1/3$ of the characteristic horizontal scale σ for longer than $\tau/3$ and all gliders maintained near their maximum speed. The time and space scales of velocity in the shallower ASAP 2006 region were expected to be smaller than the temperature scales found farther offshore in the region by Ramp et al. (2009), so the control problem was to keep gliders moving along the boundary in their sector and to keep them separated by more than 4–5 km.

The topological difference between the Slocums' closed ideal tracks and the Sprays' line segment tracks was reflected in the differences in coping with currents. The Slocum tracks have enough flexibility (shape, location, sense of rotation) to permit adapting to fairly strong currents. But Sprays, trapped on a line, had few options to deal with currents. Although the horizontal flow, being approximately geostrophic, is weakly divergent, the along-track velocity on the boundary is divergent/convergent on the eddy scale σ and near corners where straight flow produces an along-track divergence. This encourages clumping of gliders. Cross-track flow causes an on-track glider to slow, destroying interglider synchronization and generally reducing sampling power. When currents exceed a glider's through-water speed, it can be pushed off the line and out of the control volume. If currents were either steady or predictable, a feedback system might be designed to cope with currents, but the real-time ASAP data-assimilating models were unable to predict the velocity features that most affected maintaining the boundary array.

The ASAP currents, particularly deep currents off the continental shelf, often exceeded the Spray's speed, so the challenge in maintaining the boundary array was fighting these currents, not maximizing sampling performance under perfect control. Because the criteria for good sampling coverage were so simple for the Sprays and a human could make reasonable short-range current forecasts from the gliders' own observations, it was decided early to use the aid of an experienced pilot to adaptively adjust the timing of course reversals when needed by updating waypoints sent to the Sprays. The pilot was able to combine the tasks of anticipating currents, maximizing sampling performance in the short range, and minimizing the chances that unforecast currents would disrupt the array in the longer range. The Spray's onboard ability to autonomously steer relative to the current and the assigned track as well as relative to programmed waypoints was an important aid in fighting fast-changing currents.

4. GLIDER OPERATION RESULTS

4.1. Summary of Glider Fleet Operations

During the 2006 ASAP field experiment, all 10 Spray and Slocum gliders moved and sampled as planned, collecting profiles continuously except for a few premature recoveries and intermittent lapses. The profile times for all gliders are plotted in Figure 7; profiles in the gray-shaded area were collected by a glider under automatic control of the GCCS. The four Spray gliders were deployed from Moss Landing, inside Monterey Bay, starting July 21 and did not come out of the water until September 2. The six Slocum gliders were deployed from Santa Cruz just outside the eastern corner

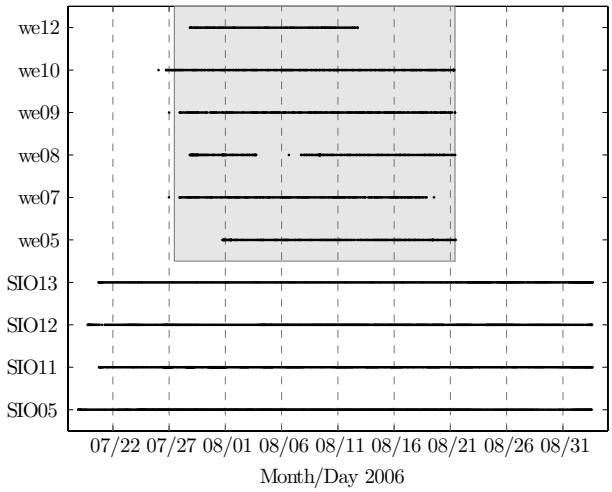

Figure 7. Times of glider profiles collected during the 2006 ASAP field experiment. Profiles in the gray box were collected by a glider under automatic control of the GCCS.

of the ASAP mapping domain starting July 27, and all six were in the water by August 1. The gap in the profile collection of glider we08 corresponds to the period of time in the first week of August that we08 was out of the water after a leak was detected. Glider we12 stopped collecting profiles when it was recovered on August 12 after a rudder-fin failure. Glider we07 was put under manual control on August 19 when it detected a water leak. GCCS control of the remaining Slocum gliders was terminated on August 21 because of concerns that all of the Slocum gliders were susceptible to leaks. The Slocum gliders were recovered by August 23.

Over the course of the experiment the Spray gliders produced 4,530 profiles. The Slocum gliders covered a 3,270-km trackline and produced 10,619 profiles. The profile locations for both Spray and Slocum gliders are shown in Figure 8. The four Spray gliders adhered primarily to the tracks along the boundary of the sampling domain in accordance with the default plan of Figure 3(b), except for those occasions on which a Spray glider deviated from the plan because of strong flow conditions or adaptation in the experiment's second half. The profiles in Figure 8(a) outside the domain, to the north and west in particular, were collected during large deviations of a Spray glider from the desired track as a result of strong flow conditions. Some profiles south of the domain [in both Figures 8(a) and 8(b)] were collected during deployment and recovery. The first major adaptation of the default glider sampling plan is visible in Figure 8(a) where a line of Spray profiles cuts diagonally across the northwestern corner of the mapping domain. Starting early in August, this line was patrolled by Spray gliders in lieu of the original boundary because of the earlier difficulties with the strong currents in this corner. The default plan for the Sprays was adapted again late in the experiment on August 21 to cover the tracks that the Slocums had been covering before they were recovered. Evidence of this adaptation can be seen in Figure 8(a), where Spray profiles appear on tracks in the interior of the domain. Adaptations were also made to rendezvous with other platforms for comparisons.

The six Slocum gliders were controlled by the GCCS to a series of 14 GCTs that were adaptations of the default Slocum glider plan of Figure 3(a). A major adaptation is visible in Figure 8(b), where a line of Slocum profiles bisects the original middle and south tracks. Profiles on this line were collected by Slocum gliders on four smaller tracks, each half as large as an original track. The tracks were created so gliders might be able to detect cold water upwelling over the top of the canyon head in the south-central portion of the mapping domain. Slocum gliders were assigned to the four new tracks during the period August 11–16.

4.2. Summary of Ocean Conditions

The ocean circulation during the 2006 ASAP field experiment consisted of the following two transitions: from upwelling to relaxation and, then, from relaxation to upwelling (for more details, see Ramp et al., 2010). A snapshot of the depth-averaged flow in the mapping domain during the relaxation-to-upwelling transition is shown in Figure 9(a). A snapshot of upwelling flow is shown in Figure 9(b). Both snapshots were generated from Spray and Slocum depth-averaged flow estimates using OA with decorrelation lengths $\sigma = 22$ km and $\tau = 2.2$ days. The flow is assumed to have zero mean and unit variance. During the bifurcating flow condition shown in Figure 9(a), it was particularly challenging to keep gliders in the domain. Gliders in the northern half of the domain were advected north and west, and gliders in the southern half of the domain were advected south and east. The flow snapshot in Figure 9(b) shows equatorward flow indicative of upwelling activity.

4.3. Results of Spray Glider Operations

Spray operations were uneventful except early in the experiment (July 27–August 10), when strong poleward currents over the continental slope made it very difficult to keep the gliders entering that area from being blown poleward out of the control volume. This poleward motion, presumably a meander or eddy in the California Undercurrent, was unpredicted by the ASAP ocean models (which then were operating without much in situ data) and was not even successfully nowcast after it had been sampled by two gliders. The operational issue was that Sprays in the western corner of the control volume could, at best, remain stationary in this current by swimming equatorward at the maximum speed for which they were ballasted. The issue of how to adapt the sampling array to compensate for loss of mobility

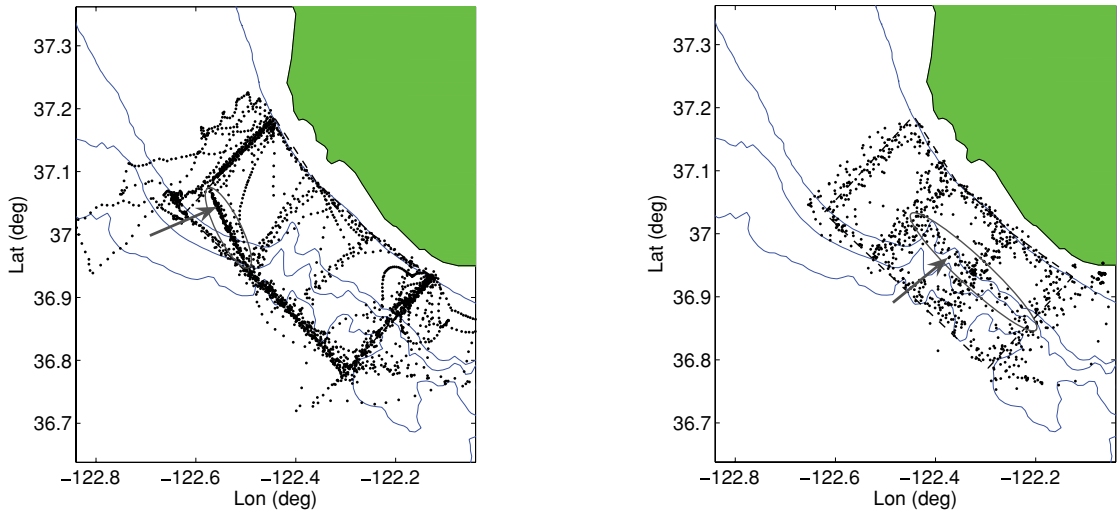

(a) Spray gliders (b) Slocum gliders

Figure 8. Location of glider profiles collected during the 2006 ASAP field experiment. (a) Spray gliders collected profiles primarily on the boundary of the ASAP domain. Profiles north or west of the domain were collected during large, current-induced deviations from the desired track. Profiles collected along the modified domain boundary are contained in a gray ellipse marked with an arrow. (b) Slocum gliders collected profiles inside the mapping domain and on its boundary. Profiles collected over the canyon head are contained in a gray ellipse marked with an arrow.

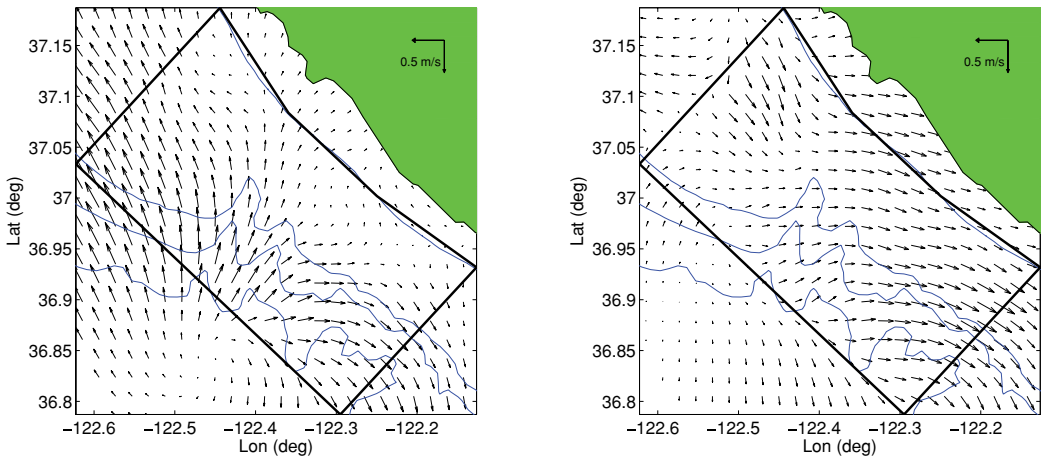

(a) 17:00 GMT August 8 (b) 00:00 GMT August 11

Figure 9. Snapshots of ocean flow as computed from glider depth-averaged flow estimates using OA. (a) Flow transition from relaxation to upwelling advected gliders out of the mapping domain; (b) equatorward flow indicative of an upwelling.

in the western corner, or how to direct the gliders around the offending current, was the subject of discussions among all the team members, but no solution was found until the current weakened.

4.4. Results of Slocum Glider Operations

Strong and highly variable flow conditions such as the ones shown in Figure 9 presented a major challenge to steering the gliders along their assigned tracks with the

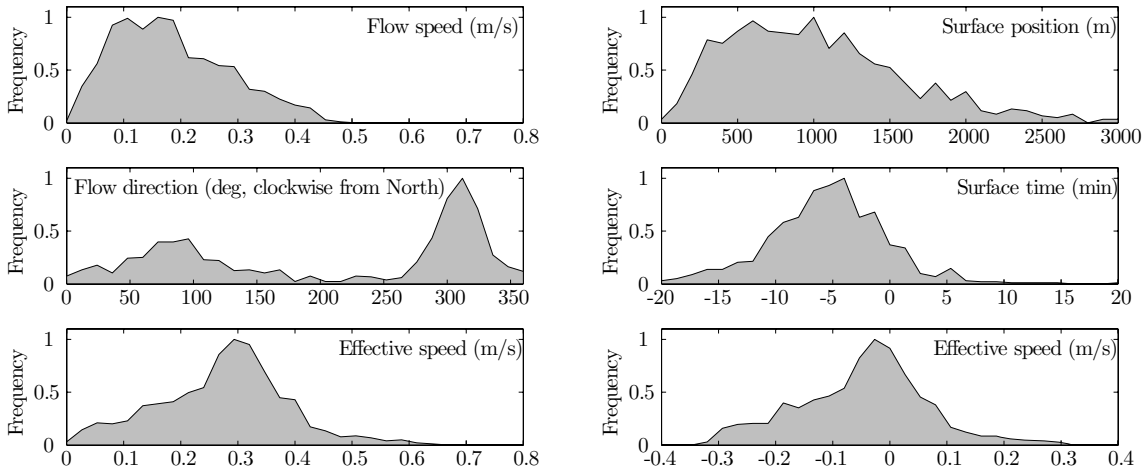

(a) Glider speed and flow velocity

(b) Error in GCCS (real-time) prediction

Figure 10. Flow velocity and GCCS prediction accuracy during the 2006 ASAP field experiment. Each frequency distribution has been normalized by the frequency of its mode so that the maximum value is 1; the plots describe probability distributions with constant scaling factors. (a, top) Depth-averaged flow speed estimated by Slocum gliders during period of GCCS activity; (a, middle) distribution of depth-averaged flow directions is bimodal: flow was predominantly poleward with less frequent onshore component; (a, bottom) Slocum glider effective speed ranged from zero to more than 0.6 m/s. (b, top) GCCS errors in predicting Slocum glider surface position; (b, middle) distribution of GCCS errors in predicting Slocum glider surface time shows a negative bias of 5 min; (b, bottom) distribution of errors between Slocum glider effective speed and GCCS prediction (0.32 m/s).

desired spacing. Plotted in the top two panels of Figure 10(a) are the frequency distribution of flow speed and direction, respectively, measured by the Slocum gliders during the period of GCCS activity from July 27 to August 21. Approximately 80% of the measured flow speeds were less than 0.27 m/s. However, 10% of the measured flow speeds exceeded 0.32 m/s, which is the Slocum glider effective speed predicted by the GCCS. The frequency distribution of flow direction is bimodal: the most common flow direction was poleward (along the shore), and the second-most common flow direction was onshore. This suggests that upwelling activity—characterized by equatorward flow—was relatively weak.

The frequency distribution of Slocum glider effective speed is shown in the bottom panel of Figure 10(a). The mode of this distribution is 0.3 m/s. Effective speeds less than 0.3 m/s occurred more frequently than effectives speeds greater than 0.3 m/s. This implies that Slocum gliders spent more time traveling against the flow than they spent traveling with it.

Strong and highly variable flow generates large errors in the GCCS prediction of where and when a glider will surface. Plotted in the top two panels of Figure 10(b) are the frequency distributions of errors in the GCCS prediction of glider surface position and time. Approximately 80% of the surface position errors were less than 1.6 km. However, 10% of the surface position errors exceeded 2 km. The frequency distribution of errors in surface time shows a negative bias of 5 min. That is, the most frequent error in the GCCS prediction of when a glider would surface was 5 min later than the actual surface time. Despite this bias, 80% of the surface time errors were less than 10.7 min. Plotted in the bottom panel of Figure 10(b) is the frequency distribution of errors in predicting effective speed, which is the difference between glider effective speed and the GCCS prediction of 0.32 m/s.

A timeline of the 14 GCTs used during the 2006 ASAP field experiment is shown in Figure 11; they are GCTs 1–15 as GCT 13 was never used. Some GCTs lasted less than a day; the longest GCT lasted 4.1 days (GCT 11). During each GCT, the GCCS automatically coordinated three to six Slocum gliders to converge to motion around their assigned tracks with the desired relative spacing. GCTs 1–3 were used to transition the Slocum gliders from their initial deployment location into the default Slocum sampling pattern shown in Figure 3(a). GCT 1 assigned glider we10 to the north track, glider we09 to the middle track, and glider we07 to the south track so that all moved synchronously in the counterclockwise direction around their tracks. When gliders we08 and we12 were deployed, a switch was made to GCT 2 [Figure 5(a)], which assigned we08 to the north track opposite we10 and we12 to the middle track opposite we09; GCT 2 assigned gliders we08, we09, we10, and we12 to coordinate to the default pattern and we07, the lone glider on the south track, to move independently about its track. During GCT 1, a strong northward flow was

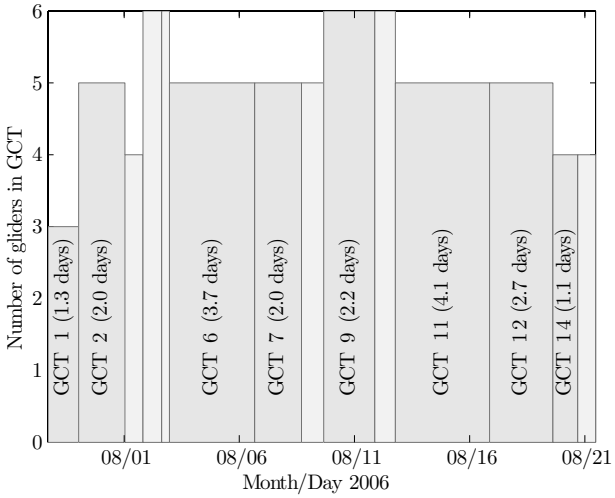

Figure 11. Time of GCTs for Slocum gliders.

observed along the northern edge of the sampling domain. By July 30, during GCT 2, this had subsided a bit, but the northward flow had strengthened in the southeastern portion of the sampling domain in excess of 25 cm/s. Indeed, glider we09 was subject to this flow while crossing the middle track when it reached an effective speed of more than 50 cm/s.

On August 1, a switch was made to GCT 3 when glider we08 detected a leak and was put under manual control. In GCT 3 glider we12 was reassigned from the middle to the north track in place of we08 and coordinated to move opposite to we10. Furthermore, we09 on the middle track and we07 on the south track were redirected to move in synchrony in the clockwise direction (rather than counterclockwise) around their tracks in an effort to take advantage of the strong northward flow on the offshore, south-central side of the sampling domain. GCT 4 began when glider we05 was deployed and we08 was put back under GCCS control; we05 and we08 were assigned to the south track and we07 moved up to the middle track opposite we09. All six gliders were coordinated according to the default plan but with motion in the clockwise direction as the strong northward flow along the offshore edge of the domain continued to intensify. Because of the strong flow, gliders we10 and we12 on the north track became too close to one another. In response, a switch was made to GCT 5: glider we10 was turned around to move in the counterclockwise direction until the glider separation increased. This GCT lasted only part of a day, and then the direction of glider we10 was reversed in GCT 6. Glider we08 was recovered during GCTs 6–8 to address the detected leak.

Adaptations in GCTs 6–9 correspond to redirection of gliders in response to changes in the ocean flow (and also redeployment of glider we08). Adaptations in GCTs 10–14 were made in response to the ASAP team decision to increase sampling density over the head of the canyon. Additionally, GCT 11 accommodated the recovery of glider we12 on August 12 and GCT 14 accommodated the change to manual control of glider we07 on August 19.

In GCT 15, one of the half-size tracks was moved offshore as part of an adaptation decided by the team to increase sampling density around an eddy that was moving offshore. This was one of the decisions that prompted an on-demand application of the glider prediction tool described in Section 3.2.3. Because of the strong southward currents in the southernmost corner of the ASAP mapping domain, there was concern that we05 would be blown south outside the box. However, the predictions based on simulations in the JPL/ROMS forecast and the NCOM/ICON forecast suggested that all would be well. Indeed we05 stayed on its coordinated trajectory during GCT 15.

5. PERFORMANCE OF COORDINATED GLIDER FLEET

In this section we examine the performance of the coordinated control of the glider fleet in the 2006 ASAP field experiment. We are interested in the impact on sampling performance of strong flow and the responsive adaptations. In the case of the Slocum glider fleet, we also consider the impact of the flow and the GCCS prediction errors on the coordination performance. Coordination performance measures the degree to which the gliders achieved the configuration specified in the GCTs. Because the GCTs were designed to collect measurements with sufficient spatial and temporal separation, good (respectively, poor) coordination results in good (respectively, poor) sampling performance.

5.1. Coordination Performance of Slocum Gliders

The performance of the GCCS in coordinating the six Slocum gliders is examined in this section using *tracking error* and *spacing error* illustrated in Figure 12 and defined as follows.

Definition 1 Tracking error *The tracking error of a glider at time t is the shortest distance between the glider and its assigned track at time t.*

The tracking error of a glider is a measure of its track-following accuracy only if the closest point on the track is where the glider is trying to go. The tracking error may not be a good metric for a glider in the interior of a very skinny track, when the closest point on the track is actually on the opposite side of where it is trying to go. Such a situation did not occur during the ASAP field experiment.

The notion of curve phase is needed to define spacing error. Consider the closed curve that defines a track with perimeter of length Ω. The curves used in the ASAP field experiment are all superellipses (Paley, 2007). Let R_k be a point on the track. The curve phase ψ_k of the point R_k is the

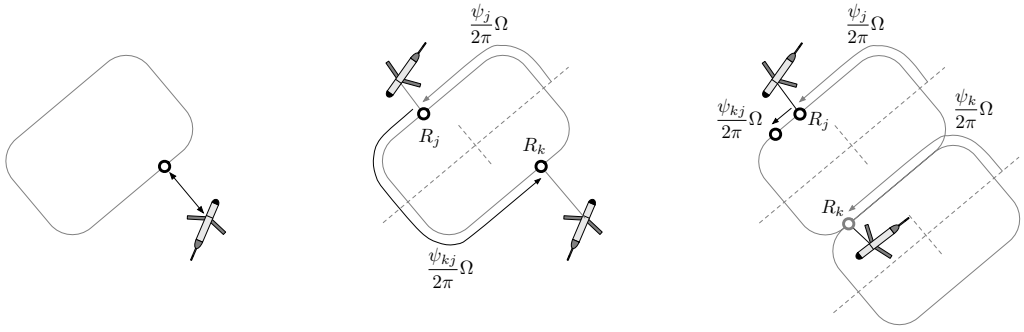

(a) Tracking error (b) Intratrack relative spacing (c) Intertrack relative spacing

Figure 12. Coordination performance metrics. (a) Tracking error is the shortest distance between a glider and its assigned track. (b) Spacing error between two gliders on the same track is proportional to the difference between the desired and actual curve phase measured between the gliders along the track (in this case the desired relative curve phase is π). Spacing error is illustrated here by the relative spacing $(\psi_{kj}/2\pi)\Omega$ of points R_k and R_j, where Ω is the track perimeter. (c) Spacing error between two gliders on different tracks is proportional to the difference between the desired and actual curve phase of point R_k relative to R_j (in this case the desired relative curve phase is 0).

arc length along the track from a fixed reference point to the point R_k in the counterclockwise direction divided by the track perimeter Ω and multiplied by 2π.

Definition 2 Spacing error *Consider two gliders labeled k and j. Suppose the gliders are assigned to tracks* 1 *and* 2*, respectively, with a desired relative curve phase $\bar{\psi}_{kj}$; tracks* 1 *and* 2 *must have the same perimeter length, but they may have different shapes, locations, or orientations. Let R_k denote the point on track* 1 *closest to glider k at time t and R_j denote the point on track* 2 *closest to glider j at time t. The spacing error between gliders k and j at time t is a number in* $[0, 1]$ *defined by*

$$|(\psi_{kj} - \bar{\psi}_{kj} + \pi) \bmod (2\pi) - \pi|/\pi, \tag{2}$$

where $\psi_{kj} := \psi_k - \psi_j$ is the curve phase ψ_k of R_k relative to the curve phase ψ_j of R_j.

Using these metrics, the overall Slocum tracking and spacing performance was best in benign currents and worst in strong currents. We provide a description of Slocum performance during GCTs 6–11; for a complete description of Slocum performance, see Paley (2007). During GCT 6, the GCCS steered five gliders around three tracks as shown in Figure 13(a). Gliders we10 and we12 were assigned to travel clockwise around the north track with relative curve phase π, we07 and we09 were assigned to travel clockwise around the middle track with relative curve phase π, and we05 was assigned to travel clockwise around the south track. In addition, the specified curve phase of each glider on the north track relative to the curve phase of a glider on the middle track was zero. A snapshot of the glider trajectories and depth-averaged flow measurements for the 24 h preceding 6:00 GMT August 4 is shown in Figure 13(b). Gliders we07 and we09 have good spacing, as discussed below. The spacing error between we10 and we12 increased when we12 was pushed by a poleward current across the deep end of the north track in just two dives and, simultaneously, the progress of we10 across the shallow end of the track was impeded by poleward flow near the shore.

The poleward flow in the mapping domain became increasingly strong during GCT 6. This process, indicative of relaxation, ultimately led to adaptation of the GCT. Each glider's effective speed is shown in Figure 14, along with its depth-averaged flow measurements. The glider effective speed fluctuated around its predicted value of 0.32 m/s, ranging from more than 0.5 m/s when traveling with the flow to nearly zero when traveling against the flow. It can be observed that the effective speed was nearly zero for four of five gliders at the conclusion of GCT 6 (identified in Figure 14 by a vertical line on day 3.7). All of the gliders got stuck on the shallow end of their tracks when they tried to head equatorward against the flow. The direction of rotation of all gliders was reversed to counterclockwise in GCT 7. The idea was to take advantage of the strong poleward flow near shore and have the gliders combat the poleward flow in deep water, where it appeared weaker.

When glider forward progress was impeded by the flow, coordination performance deteriorated. Plotted for GCT 6 is the tracking error in Figure 15(a) and spacing error in Figure 15(b). For the first 3 days of GCT 6, the tracking error for all of the gliders was almost always less than 2 km (the perimeter of the track was 71 km). Likewise, during this time, the intratrack spacing error of glider pairs we10/we12 and we07/we09, shown at the top in Figure 15(b), remained under 40%, and, on three occasions, dropped nearly to zero. Other than one brief spike on day 1, the intertrack spacing error of glider pairs we10/we09 and

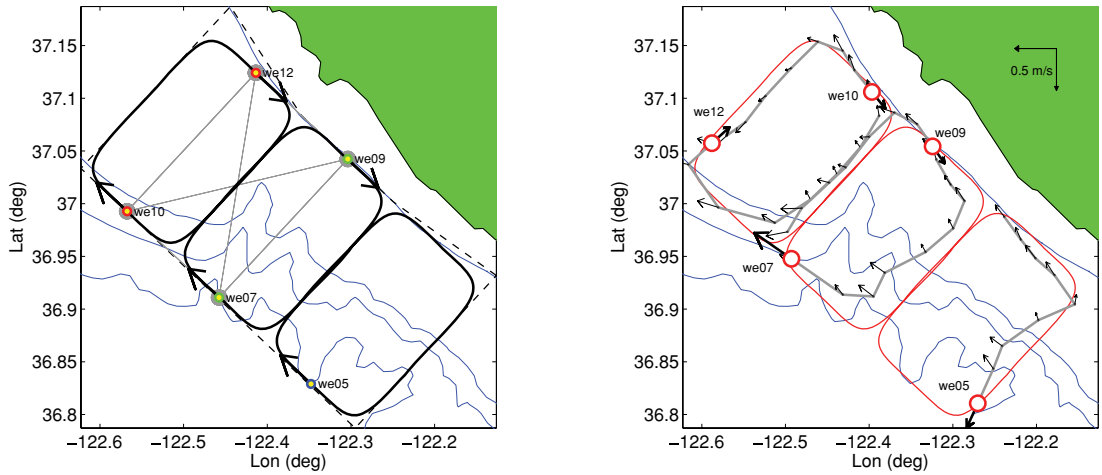

(a) ASAP GCT 6

(b) Glider trajectories, 6:00 GMT August 4

Figure 13. Slocum glider trajectories and depth-averaged flow measurements during GCT 6. (a) GCT 6. (b) Trajectories (gray lines) and flow measurements (thin black arrows) shown for 24-h period prior to 6:00 GMT August 4; each glider's effective speed is indicated by a thick black arrow. Glider coordination performance, initially good, was eventually degraded by strong poleward flow.

we07/we12 during the first 3 days also remained under 40%. Tracking and spacing errors growing above 40% on day 3 prompted us to switch the GCT.

When the gliders reversed direction of rotation under GCT 7, coordination performance partially recovered. As seen in Figure 15(a), after day 3.7 under GCT 7, the tracking error of we07 remained low and the tracking error of we09 decreased. After day 5, the spacing error of this glider pair also recovered. However, the tracking and spacing errors for gliders we10 and we12 did not recover under GCT 7, prompting the switch to GCT 8. Under GCT 8 gliders we10 and we12 were briefly sent in opposite directions around the north track to quickly recover proper separation.

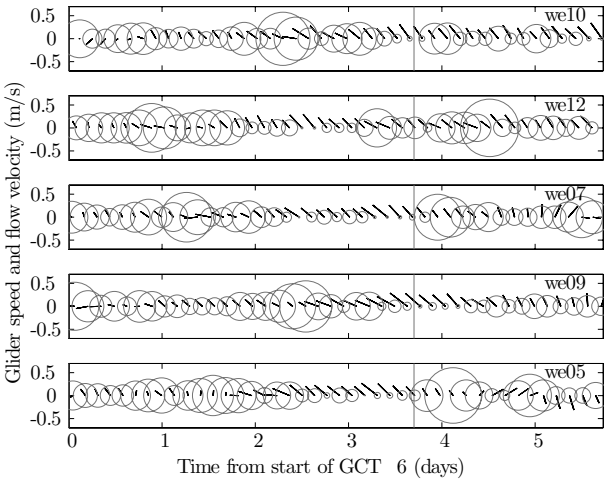

Figure 14. Slocum glider speed and depth-averaged flow velocity during GCT 6. Glider effective speed at time t is denoted by the radius of the circle centered at time t and speed 0. The depth-averaged flow velocity at time t is depicted by a black line with one end at time t and speed 0; the length of the line is the speed, and its orientation corresponds to the orientation of the flow velocity (up is north, right is east). By day 3, forward progress of all gliders had been substantially impeded by strong poleward flow, prompting adaptation of the GCT at time $t = 3.7$ days (vertical gray line).

The GCCS achieved good glider coordination performance, as quantified below, during GCT 9, which ran for 2.2 days from 16:00 GMT August 9 to 21:09 GMT August 11. GCT 9 marked the return of glider we08 to GCCS control, its leak repaired. Under GCT 9, the GCCS steered all six Slocum gliders to three tracks. The GCT specified three glider pairs—we10/we12, we07/we09, and we05/we08—to have relative curve phase of π. Each glider pair was assigned to a different track, and there was no intertrack coordination.

During GCT 9, there was moderate onshore and weak poleward flow in the west and north portions of the mapping domain, respectively. Strong equatorward flow in the southeastern corner was indicative of a transition to upwelling. Glider we08, initially located near the southern corner of the mapping domain, was advected by the flow to a location southeast of the mapping domain. As can be seen in Figure 16, the effective speed of we08 was reduced to nearly zero for more than 12 h. When we08 slowed down, we05 actually cut across the southern corner of the south track and "passed" we08, meaning that the curve phase of we05 relative to we08 changed sign. No glider other than we08 experienced prolonged interruptions of forward progress during GCT 9. Coordination performance

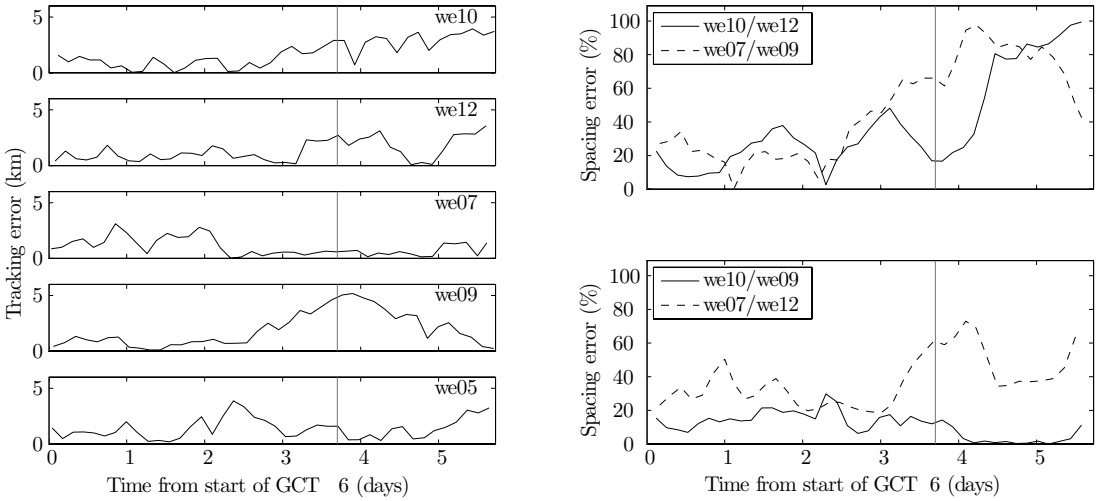

(a) Tracking error GCT 6 (b) Spacing error GCT 6

Figure 15. Coordination performance of Slocum gliders during GCT 6. The start of GCT 7 is shown by a vertical gray line at $t = 3.7$ days. (a) Until $t = 3$ days, tracking error of all gliders was less than 2 km, except for short periods; (b, top) until $t = 3$ days, intratrack spacing error remained under 40%; (b, bottom) except for one spike on day 1, intertrack spacing error from $t = 0$ days to $t = 3$ days also remained under 40%. Gliders reversed direction under GCT 7, which started at $t = 3.7$ days; we07 and we09 recovered good coordination performance, but we10 and we12 did not.

recovered during GCT 8 and remained good during GCT 9, except for gliders we05 and we08. Tracking error for the four gliders on the middle and north tracks was less than 2 km. The spacing error was below 10% for we10 and we12,

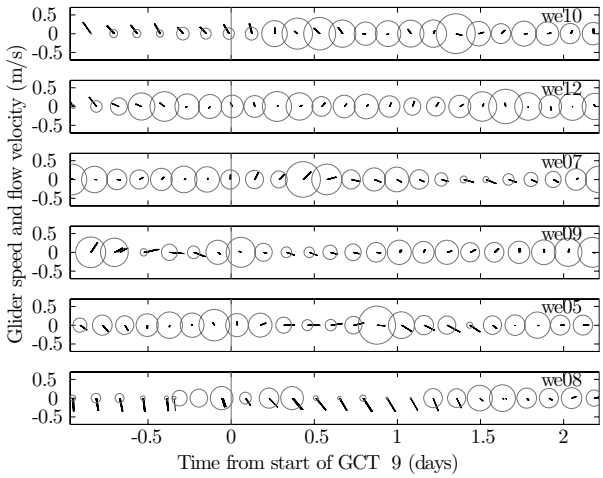

Figure 16. Slocum glider speed and depth-averaged flow velocity during GCT 9. This period of the experiment was characterized by strong equatorward flow in the southern portion of the mapping domain, which reduced nearly to zero the effective speed of we08. Moderate onshore and weak poleward flow in the middle and northern portions of the domain did not substantially impair the forward progress of gliders deployed there.

orbiting the north track in the weakest flow, whereas spacing error was between 10% and 40% for we07 and we09, orbiting the middle track in moderate, bifurcating flow. Spacing error was the worst for we05 and we08, situated on the south track in the strongest flow. Spacing error for these two gliders did recover by the end of GCT 9, after we05 passed we08 and we08 returned to the track.

The adaptation from GCT 9 to GCT 10 was initiated by an ocean science objective and affected only the two gliders on the middle track. The ASAP team proposed to split the middle track into two smaller tracks, so that gliders would sample the alongshore line bisecting the original middle track. This bisecting line follows the canyon head, the region where cold water was presumed to be emerging. The hypothesis that this was where cold water was emerging would be tested by gliders we07 and we09 collecting profiles along each of the new tracks. GCT 10, which ran for less than a day, was adapted to GCT 11 when we12 sustained a terminal failure of its rudder fin. During GCT 11, which ran for 4.1 days from 18:26 GMT August 12 to 20:47 GMT August 16, we10 orbited the north track alone. All of the other track assignments and coordination are the same in GCT 11 as in GCT 10: we07 and we09 were assigned to orbit with relative curve phase 0 the two small tracks circumscribed by the original middle track; we05 and we08 were assigned to orbit the south track with relative curve phase π.

The GCCS achieved high coordination performance during GCTs 10 and 11 in the presence of moderate, onshore flow. Other gliders experienced only mild

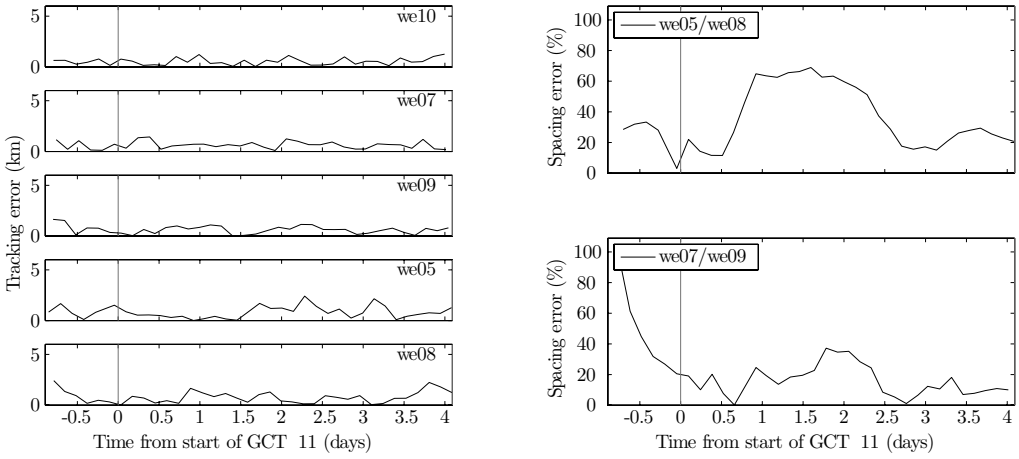

(a) Tracking error GCT 11 (b) Spacing error GCT 11

Figure 17. Coordination performance of Slocum gliders during GCT 11. (a) Except for short periods, tracking error was less than 2 km for all gliders; (b, top) intratrack spacing error between we05 and we08 experienced a surge and then recovered, when we05 was temporarily slowed; (b, bottom) intertrack spacing error between we07 and we09 decreased rapidly and remained below 40%, illustrating the "step" response to adapting GCT 9 to GCT 10.

fluctuations of effective speed. Glider we05 halted, not because of flow conditions, but because of an interruption in satellite communication. Nonetheless, tracking error for all gliders, shown in Figure 17(a), was consistently less than 2 km. The intratrack spacing error of we05 and we08, plotted in the top of Figure 17(b), experienced a temporary surge when the forward progress of we05 was impaired; it subsequently recovered to less than 30%. The intertrack spacing error of we07 and we09, shown in the bottom of Figure 17(b), decreased sharply during GCT 10 and remained below 40% during GCT 11. This figure nicely illustrates the GCCS "step" response to adaptation of the GCT from 9 to 10.[1]

5.2. Sampling Performance of Spray and Slocum Glider Fleet

The sampling performance in the domain $\mathcal{I}(t)$ and on the boundary $\mathcal{I}_\delta(t)$ are plotted as a function of time t for the Slocum gliders in Figure 18(a), for the Spray gliders in Figure 18(b), and for the combined glider fleet in Figure 18(c). In all three figures, the period when the GCCS was active, which corresponds to the period when the Slocum gliders were in the water, is colored gray. The Slocum glider sampling performance decreased when the Slocum glider coordination was poor, and it recovered when coordination performance improved.

[1]The step response of a control system is the behavior of its output when its input changes suddenly from one constant value to another; here the system is the GCCS and the inputs are the GCTs.

Figure 18(a) shows that the Slocum gliders achieved a relatively high sampling performance inside the sampling domain and on its boundary. In fact, the sampling performance inside and on the domain was nearly the same. As expected, the performance ramped up when the gliders first entered the water at the end of July and ramped down when they were recovered after August 21. During the period of time when they were in the water, the Slocum glider sampling performance was generally level, with some fluctuations. The largest downward fluctuation occurred on August 6, during GCT 6, when coordination performance suffered due to adverse flow conditions (see discussion in Section 5.1). The fact that sampling performance recovered subsequent to adaptation of the GCT shows how coordinated motion control can improve sampling performance.

For much of the experiment, Spray glider sampling performance, plotted in Figure 18(b), was distinctly higher on the boundary of the sampling domain than in its interior. This result is consistent with the Spray glider sampling plan shown in Figure 3(b), which dedicated the Spray gliders to patrolling tracks along the periphery of the domain. The only period of time during which the sampling performance was not higher on the boundary occurred after the Slocum gliders were recovered, when the Spray gliders were reassigned to tracks that sampled both the domain boundary and its interior.

The combined sampling performance of the Spray and Slocum gliders is shown in Figure 18(c). When both Spray gliders and Slocum gliders were in the water, the combined sampling performance was higher than the sampling performance of either the Spray gliders or the Slocum gliders separately, although sampling performance does not add

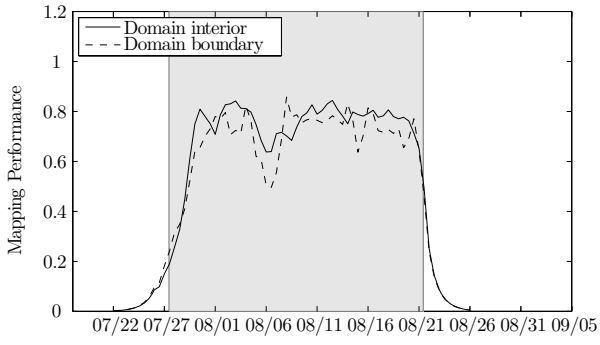

(a) ASAP FE Slocum glider sampling performance

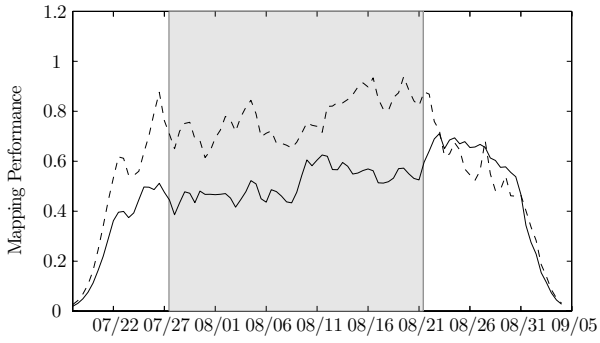

(b) ASAP FE Spray glider sampling performance

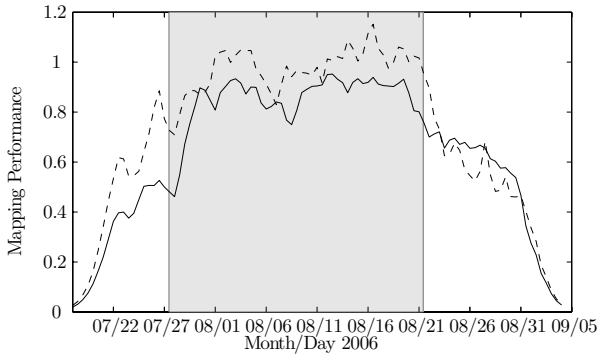

(c) ASAP FE combined glider sampling performance

Figure 18. Glider sampling performance during the 2006 ASAP field experiment (FE). The sampling performance ramped up when the gliders entered the water and ramped down when the gliders came out of the water. The portion of all three plots that is shaded gray corresponds to the period of time during which the GCCS was actively steering the Slocum gliders.

linearly. During this period of time, the combined sampling performance was higher on the boundary of the mapping domain than inside it. This observation suggests an imbalance in the distribution of gliders inside and on the boundary; combined sampling performance could have been balanced if one or more of the boundary (Spray) gliders were allocated to the interior. Some of the fluctuations in the Spray and Slocum sampling performance are visible in the combined sampling performance, although other fluctuations are visible too.

The degree to which the sampling performance of the Spray gliders reinforced and extended the sampling performance of the Slocum gliders depended on the positions and times of the Spray glider profiles relative to the positions and times of the Slocum glider profiles. The difference between the combined sampling performance and the separate sampling performances was greatest when profiles in the combined set of profiles were well distributed and not overlapping.

6. FINAL REMARKS

A fleet of 10 autonomous underwater gliders were deployed as an adaptive, coordinated ocean sampling network throughout the month of August 2006 in a 22 × 40 km domain just northwest of Monterey Bay, California, as part of the ASAP program's 2006 field experiment. The 2006 ASAP experiment demonstrated and tested an adaptive coastal ocean observing system featuring the coordinated sampling of the gliders integrated with an assortment of sensing platforms, three real-time ocean models, numerical optimization and prediction tools, a virtual control room, and a team of scientists. The control and coordination of the gliders provided autonomy and adaptability while maintaining the means to integrate humans in the loop in a supervisory role. The field experiment successfully demonstrated the methodology of Leonard et al. (2007), which uses scalable feedback control laws to coordinate the motion of robotic vehicles into sampling patterns, designed to maximize information in the data collected. The need for feedback to coordinate the gliders was clearly illustrated in the 2003 AOSN-II field experiment when it was observed that, without feedback, currents tend to drive gliders into clumps, which leads to sensing redundancy and negatively impacts sampling performance (Leonard et al., 2007).

Six Slocum gliders were autonomously controlled for 24 days straight to follow coordinated motions patterns, optimized for sampling performance. The desired motion patterns were adapted 14 times; these were the only (momentary) human-initiated interruptions of the otherwise completely automated system. Four Spray gliders were coordinated for 44 days to patrol the north, west, and south boundaries of the domain; control of the Spray gliders also used a combination of automation and human supervision, tailored to their task. The overall sampling performance of the gliders was correlated to their level of coordination. The Slocum gliders maintained coordination reasonably close to desired so that sampling was well distributed in space and time. The Spray gliders maintained well-distributed sampling on the domain boundaries. The major exceptions

were periods of strong currents, which prohibited gliders from moving where they were supposed to go. Adaptation of the glider sampling patterns was used in many of these circumstances; the adaptations were often successful in mitigating the impact of strong currents. Adaptation of the glider sampling patterns also successfully provided response to changes in ocean science objectives, including a midexperiment request for sampling over the head of the canyon, as well as response to changes in glider availability, such as when a Slocum glider was recovered for a short period because of a detected leak.

The 2006 ASAP field experience underscores some important guidelines for the design and control of glider fleets. First, coordinated control is most effective when the advecting currents are weak to moderate as compared to the platform speed. Second, in the face of stronger currents, the design should allow for gliders to change heading over a range of at least 180 deg. This flexibility was in place in the case of the Slocum gliders by means of motion pattern adaptations, and it proved to be very helpful in maintaining performance in spite of strong currents. The Spray gliders, assigned to the periphery of the sampling domain, did not have this flexibility; indeed, strong alongshore currents prevented the Spray gliders from moving near the western and southern corners. Third, although slow operational speed is needed to extend duration and make gliders economically attractive, the ability to occasionally increase this speed to deal with unusually strong currents would greatly expand the ability of gliders to make measurements where they are wanted.

The 2006 ASAP experiment demonstrated sustained and automated coordinated control, adaptation, and integrated human decision making for a fleet of underwater gliders in a challenging coastal ocean environment. The field results provide proof of concept for a new capability for ocean sampling and suggest promising opportunities for collaborative robotic sensing in other domains.

ACKNOWLEDGMENTS

We acknowledge John Lund of WHOI and Jeffrey Sherman of SIO for their important contributions to glider operations. We are grateful to Tom Curtin for his vision and to all those who participated in the ASAP program and experiment, especially our closest ASAP collaborators: Steve Ramp, Pierre Lermusiaux, Yi Chao, Igor Shulman, Sharan Majumdar, Jim Bellingham, Michael Godin, and Jerry Marsden. We thank the anonymous reviewers for their very helpful comments. This research was supported by Office of Naval Research grants N00014-04-1-0534 and N0014-02-1-0826.

REFERENCES

Bellingham, J., & Zhang, Y. (2005, November). Observing processes that vary in time and space with heterogeneous mobile networks. In Proceedings International Workshop Underwater Robotics for Sustainable Management of Marine Ecosystems and Environmental Monitoring, Genoa, Italy (pp. 9–16).

Bishop, C. H., Etherton, B. J., & Majumdar, S. J. (2001). Adaptive sampling with the ensemble transform Kalman filter. Part I: Theoretical aspects. Monthly Weather Review, 129(3), 420–436.

Bogden, P. (2001). Gulf of Maine Ocean Observing System (GOMOOS). Accessed September 7, 2010, at www.gomoos.org.

Bretherton, F. P., Davis, R. E., & Fandry, C. B. (1976). A technique for objective analysis and design of oceanographic experiments applied to MODE-73. Deep-Sea Research, 23(7), 559–582.

Chappell, S., Komerska, R., Blidberg, D., Duarte, C., Martel, G., Crimmins, D., Beliard, M., Nitzel, R., Jalbert, J., & Barton, R. (2007, August). Recent field experience with multiple cooperating solar-powered AUVs. In Proceedings 15th International Symposiam Unmanned Untethered Submersible Technology, Durham, NH.

Dickey, T. (2003). Emerging ocean observations for interdisciplinary data assimilation systems. Journal of Marine Systems, 40–41, 5–48.

Fiorelli, E., Leonard, N., Bhatta, P., Paley, D., Bachmayer, R., & Fratantoni, D. (2006). Multi-AUV control and adaptive sampling in Monterey Bay. IEEE Journal of Oceanic Engineering, 31(4), 935–948.

Gandin, L. S. (1965). Objective analysis of meteorological fields. Jerusalem: Israel Program for Scientific Translations.

Glenn, S., Jones, C., Twardowski, M., Bowers, L., Kerfoot, J., Kohut, J., Webb, D., & Schofield, O. (2008). Glider observations of sediment resuspension in a Middle Atlantic Bight fall transition storm. Limnology and Oceanography, 53(5, Part 2), 2180–2196.

Godin, M., Bellingham, J., Rajan, K., Leonard, N., & Chao, Y. (2006, September). A collaborative portal for ocean observatories. In Proceedings of MTS/IEEE Oceans, Boston, MA.

Graham, W. M., & Largier, J. L. (1997). Upwelling shadows as nearshore retention sites: The example of northern Monterey Bay. Continental Shelf Research, 17(5), 509–532.

Grocholsky, B. (2002). Information-theoretic control of multiple sensor platforms. Ph.D. thesis, University of Sydney.

Haddock, S., & Fratantoni, D. (2009). Introduction to the Autonomous Ocean Sampling Network (AOSN-II) program. Deep-Sea Research II, 56, 61.

Jakuba, V., & Yoerger, D. R. (2008, December). Autonomous search for hydrothermal vent fields with occupancy grid maps. In Proceedings Australasian Conference on Robotics and Automation, Canberra, Australia.

Leonard, N., Paley, D., Lekien, F., Sepulchre, R., Fratantoni, D., & Davis, R. (2007). Collective motion, sensor networks, & ocean sampling. Proceedings of the IEEE, 95, 48–74.

Leonard, N., Ramp, S., Davis, R., Fratantoni, D., Lermusiaux, P., Marsden, J., & Schmidt, H. (2006). Adaptive Sampling and Prediction (ASAP) Annual Report. Office of Naval Research.

Lermusiaux, P. F. J. (1999). Data assimilation via error subspace statistical estimation, Part II: Mid-Atlantic Bight shelfbreak front simulations, and ESSE validation. Monthly Weather Review, 127(8), 1408–1432.

Lermusiaux, P. F. J., & Robinson, A. R. (1999). Data assimilation via error subspace statistical estimation, Part I: Theory and schemes. Monthly Weather Review, 127(8), 1385–1407.

Maczka, D., & Stilwell, D. (2007, September). Experiments in distributed navigation for AUV platoons. In Proceedings IEEE/MTS OCEANS, Alberta, Canada.

Majumdar, S. J., Bishop, C. H., & Etherton, B. J. (2002). Adaptive sampling with the ensemble transform Kalman filter. Part II: Field program implementation. Monthly Weather Review, 130(5), 1356–1369.

Olivieri, R. A., & Chavez, F. P. (2000). A model of plankton dynamics for the coastal upwelling system of Monterey Bay, California. Deep-Sea Research II, 47(5), 1077–1106.

Paley, D. (2007). Cooperative control of collective motion for ocean sampling with autonomous vehicles. Ph.D. thesis, Princeton University.

Paley, D., Zhang, F., & Leonard, N. (2008). Cooperative control for ocean sampling: The glider coordinated control system. IEEE Transactions on Control Systems Technology, 16(4), 735–744.

Pilskaln, C. H., Paduan, J. B., Chavez, F. P., Anderson, R. Y., & Berelson, W. M. (1996). Carbon export and regeneration in the coastal upwelling system of Monterey Bay, central California. Journal of Marine Research, 54(6), 1149–1178.

Princeton University (2006a). Glider Coordinated Control System (GCCS): Glider planner and status. Accessed September 7, 2010, at http://www.princeton.edu/dcsl/asap/images/gplan_latest.shtml.

Princeton University (2006b). Glider Coordinated Control System (GCCS): Glider prediction. Accessed September 7, 2010, at http://www.princeton.edu/~dcsl/asap/prediction/Prediction.shtml.

Princeton University (2006c). Glider Coordinated Trajectories Markup Language (GCTML) and Optimizer Interface. Accessed September 7, 2010, at http://orca.princeton.edu/gctml/.

Rahimi, M., Pon, R., Kaiser, W. J., Sukhatme, G. S., Estrin, D., & Srivastava, M. (2004, April). Adaptive sampling for environmental robotics. In Proceedings 2004 IEEE International Conference Robotics and Automation, New Orleans, LA (vol. 4, pp. 3537–3544).

Ramp, S., Davis, R., Leonard, N., Shulman, I., Chao, Y., Robinson, A., Marsden, J., Lermusiaux, P., Fratantoni, D., Paduan, J., Chavez, F., Bahr, F., Liang, S., Leslie, W., & Li, Z. (2009). Preparing to predict: The Second Autonomous Ocean Sampling Network (AOSN-II) experiment in Monterey Bay. Deep-Sea Research II, 56, 68–86.

Ramp, S., Lermusiaux, P., Shulman, I., Chao, Y., Wolf, R., & Bahr, R. (2010). Oceanographic and atmospheric conditions on the continental shelf north of the Monterey Bay during August 2006. In preparation.

Ramp, S. R., Paduan, J. D., Shulman, I., Kindle, J., Bahr, F. L., & Chavez, F. (2005). Observations of upwelling and relaxation events in the northern Monterey Bay during August 2000. Journal of Geophysical Research—Oceans, 110(C7), C07013.

Richards, A., Bellingham, J., Tillerson, M., & How, J. (2002, August). Co-ordination and control of multiple UAVs. AIAA Guidance, Navigation, and Control Conference, Monterey, CA.

Robinson, A. (1999). Forecasting and simulating coastal ocean processes and variabilities with the Harvard Ocean Prediction System. In C. Mooers (ed.), Coastal ocean prediction (pp. 77–100). Washington, DC: American Geophysical Union.

Robinson, A., & Glenn, S. (1999). Adaptive sampling for ocean forecasting. Naval Research Reviews, 51(2), 28–38.

Rosenfeld, L. K., Schwing, F. B., Garfield, N., & Tracy, D. E. (1994). Bifurcated flow from an upwelling center: A cold water source for Monterey Bay. Continental Shelf Record, 14(9), 931–964.

Rudnick, D., Davis, R., Eriksen, C., Fratantoni, D., & Perry, M. (2004). Underwater gliders for ocean research. Marine Technology Society Journal, 38(1), 48–59.

Schofield, O., Bergmann, T., Bissett, P., Grassle, J., Haidvogel, D., Kohut, J., & Glenn, S. (2002). The long-term ecosystem observatory: An integrated coastal observatory. IEEE Journal of Oceanic Engineering, 27, 146–154.

Schulz, B., Hobson, B., Kemp, M., & Meyer, J. (2003, September). Field results of multi-UUV missions using Ranger micro-UUVs. In Proceedings OCEANS 2003 MTS/IEEE Conference, San Diego, CA (vol. 2, pp. 956–961).

Sepulchre, R., Paley, D. A., & Leonard, N. E. (2007). Stabilization of planar collective motion: All-to-all communication. IEEE Transactions on Automatic Control, 52(5), 811–824.

Sepulchre, R., Paley, D. A., & Leonard, N. E. (2008). Stabilization of planar collective motion with limited communication. IEEE Transactions on Automatic Control, 53(3), 706–719.

Shchepetkin, A., & McWilliams, J. (2004). The Regional Oceanic Modeling System: A split-explicit, free-surface, topography-following-coordinate ocean model. Ocean Modelling, 9, 347–404.

Sherman, J., Davis, R., Owens, W., & Valdes, J. (2001). The autonomous underwater glider "Spray." IEEE Journal of Oceanic Engineering, 26(4), 437–446.

Shulman, I., McGillicuddy, D. J., Jr., Moline, M. A., Haddock, S. H. D., Kindle, J. C., Nechaev, D., & Phelps, M. W. (2005). Bioluminescence intensity modeling and sampling strategy optimization. Journal of Atmospheric and Oceanic Technology, 22(8), 1267–1281.

Shulman, I., Wu, C.-R., Lewis, J. K., Paduan, J. D., Rosenfeld, L. K., Kindle, J. D., Ramp, S. R., & Collins, C. A. (2002). High resolution modeling and data assimilation in the Monterey Bay area. Continental Shelf Research, 22(8), 1129–1151.

Smith, R., Chao, Y., Li, P., Caron, D., Jones, B., & Sukhatme, G. S. (2010). Planning and implementing trajectories for autonomous underwater vehicles to track evolving ocean processes based on predictions from a regional ocean model. International Journal of Robotics Research (in press).

Suzuki, M. T., Preston, C. M., Chavez, F. P., & DeLong, E. F. (2001). Quantitative mapping of bacterioplankton populations in seawater: Field tests across an upwelling plume in Monterey Bay. Aquatic Microbial Ecology, 24(2), 117–127.

Thomson, R. E., Mihaly, S. F., Rabinovich, A. B., McDuff, R. E., Veirs, S. R., & Stahr, F. R. (2003). Plume-induced topographically constrained circulation at Endeavour Ridge: Implications for the colonisation of deep hydrothermal vents. Nature, 424, 545–549.

Webb, D., Simonetti, P., & Jones, C. (2001). SLOCUM: An underwater glider propelled by environmental energy. IEEE Journal of Oceanic Engineering, 26(4), 447–452.

Willcox, J. S., Bellingham, J. G., Zhang, Y., & Baggeroer, A. B. (2001). Performance metrics for oceanographic surveys with autonomous underwater vehicles. IEEE Journal of Oceanic Engineering, 26(4), 711–725.

Zhang, F., Fratantoni, D. M., Paley, D. A., Lund, J. M., & Leonard, N. E. (2007). Control of coordinated patterns for ocean sampling. International Journal of Control, 80(7), 1186–1199.

Zhong, L., & Li, M. (2006). Tidal energy fluxes and dissipation in the Chesapeake Bay. Continental Shelf Research, 26(6), 752–770.